Study of failure cases for the LHC dilution system

Bachelor Thesis

Lea Richtmann

November 29, 2018

Supervisor: Prof. Dr. Christian Ospelkaus
Dr. Christoph Wiesner (CERN)

Leibniz Universität Hannover
Faculty of Mathemathics and Physics

Abstract

The dilution system of the LHC beam dump system is used to distribute the energy deposition at the dump block for every beam dump. In this work, failure scenarios like partially lost dilution or changes in the beam sweep path due to erratic firing of the dilution kicker magnets are investigated. The implications these failure cases could have for upgraded horizontal kickers from Run 3 on are studied. The upgraded kicker magnets maintain the bunch density at the dump or give even some improvements. Furthermore, a change in the kicker waveforms is analyzed with the conclusion that the new kicker waveforms should be maintained. A last part examines the sensitivity of bunch density to the LHC filling scheme showing that only the beam entrance window of the dump is very sensitive to the used filling scheme.

Contents

1 Introduction and Motivation

Particle accelerators are used to bring charged particles to very high energies. These highly energetic particles can then be brought into collisions to study new particles created during these collisions and thus improve our understanding of the composition and behavior of matter.

The Large Hadron Collider (LHC) at the European Organization for Nuclear Research (CERN) is the particle accelerator with highest energy in the world. In the main operation mode, two proton beams are accelerated to 99.999 999 % the speed of light and collide at four interaction points. From 2019 on, the LHC will be upgraded. After the Long Shutdown 2 2019/2020 the LHC will start its Run 3 working with protons at an energy of 7 TeV during probably three years. This period will be followed by the Long Shutdown 3 from 2024-2026 during which further works will be undertaken to upgrade the accelerator to the High Luminosity LHC (HL-LHC) resulting in an increase in particle collisions corresponding to 5 to 7 times the nominal luminosity [5].

The total stored energy in each of the two LHC beams is currently about 336 MJ and will increase to 724 MJ for the HL-LHC upgrade (2808 proton bunches, currently: bunch intensity 1.15×10^{11} protons at an energy of 6.5 TeV, HL-LHC: bunch intensity 2.3×10^{11} protons at an energy of 7 TeV [3, p. 469]). After their normal circulating time of around ten hours or if something unexpected happens during operation, the safe extraction and dump of the beam has to be ensured. This means that, independently of the beam energy at any given moment there must be the possibility to remove all the protons from the machine without causing any damage. A complex beam dump system is needed in order to satisfy these operational requirements. The system involves the extraction of the beam out of its nominal orbit to separated dump lines about 1 km long at the end of which the protons get absorbed by an 8 m long graphite block.

Even if the proton beam widens at the dump block, its width is still only around two millimeters. This concentration means a very high energy density. If the concentrated proton beam were to hit graphite, it would penetrate it for 25 m and damage it [17]. This fact shows that a dilution system is needed to safely dump the beam without causing damages.

The dilution is executed by means of pulsed magnets that sweep the beam over the front-face of the dump block in order to distribute its energy deposition. Even with this dilution, currently the graphite dump can reach peak temperatures around 1000 °C during a nominal beam dump. For HL-beams these temperatures are assumed to rise even to 1860 °C [20]. This is a strong increase in temperature especially when bearing in mind that it is assumed that the material has a survival temperature of 3000 °C [10]. If a part of the dilution system were to fail the energy deposition would be more concentrated which could lead to critical rises of temperature and thermo-mechanical stresses for the dump.

All this leads to the need to study in detail the implications of failures of the dilution system which is the purpose of this work.

The first part gives an introduction to the relevant concepts of accelerator physics as well as to the LHC and its beam dump system (chapter 2). This is followed by a description of the Python code used and benchmarking of tools for the analysis (chapter 3). The main part includes the different studies: The dilution patterns and the formation of the density of proton bunches at the dump is analyzed for different scenarios (chapter 4.1). Furthermore, studies were performed analyzing the effect of upgraded horizontal dilution kickers (chapter 4.2), the effect of a change in the damping factor of the damped-sine-like magnet currents (chapter 4.3) and about the sensitivity of the energy deposition with respect to the LHC filling scheme (chapter 4.4).

2 Physical Background

2.1 Accelerator Physics: Relevant concepts

Circular particle accelerators have two main components: Electrical fields for acceleration and magnetic fields for changing the beam path and focusing.

A particle with charge q that is moving with velocity $\vec{v}$ in a magnetic field $\vec{B}$ and an electric field $\vec{E}$ is subject to the Lorentz force

$$\vec{F} = q(\vec{v} \times \vec{B} + \vec{E}) \tag{1}$$

The force is perpendicular to the particle's velocity and to the magnetic field, meaning that the particle's path gets bent through the magnetic part of the force. In addition to that the magnetic part of the force is proportional to the particle's velocity. To achieve the same magnitude of force an $\vec{E}$-field must thus be much stronger than the $\vec{B}$-field. This is why in colliders with high energies magnets are used to keep the particles on their circular path and more generally in any moment when it is needed that the particles change their direction.

In a homogeneous field a whole beam of particles receives the same Lorentz force. This explains why the homogeneous field of dipoles is used to bend the whole beam to keep it on a circular trajectory. In an inhomogeneous field, however, the behavior of a particle beam cannot be studied as a collective bending: Each particle will receive a slightly different force according to its individual position in the field. The behavior of the beam as a whole will then depend on the type of field the particles are going through. One example of inhomogeneous magnetic fields that is relevant for this work are quadrupoles (see Figure 1): The field of a quadrupole is a gradient field; that is, it is stronger in the outer parts than in the inner parts. This results in

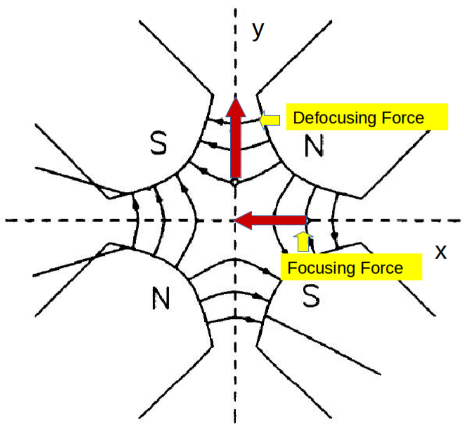

Figure 1: The field of a magnetic quadrupole and the forces executed on a charged particle, modified from [23, p. 65]

a focusing force and thus quadrupoles are used for focusing the beam in colliders: Particles that are further away from the center feel a stronger field and are thereby pulled back to the design orbit, particles in the center are in a field free region and do not change their position. However, a quadrupole only focuses in one plane while it defocuses in the perpendicular plane (see Figure 1). To compensate for this effect, two quadrupoles with their fields turned by 90° are set one after each other with a drift in between resulting in so-called FODO-cells [18, p. 104ff.].

As explained, the quadrupole field is stronger further away from the center. This means that, if a particle goes through a point far away from the center of a quadrupole field in the direction in which it is defocusing (for example for the field shown in Figure 1 in the y-direction) it gets bent further away from its center. A whole particle beam travelling through these outer parts of a quadrupole gets kicked away from its nominal orbit.

As particles in colliders are travelling with relativistic velocities the Lorentz factor is needed. For highly energetic particles that travel with a velocity close to the speed of light ($v \approx c$) the Lorentz factor γ can be determined using the particle's total and rest energy.

The particle's total energy $E_{tot} = \gamma m_0 c^2$, with m_0 being the particle's rest mass, is normally known for particles in accelerators as it is the accelerator's design energy, to which the particles are accelerated. The rest energy is determined by $E_0 = m_0 c^2$. As the total energy and the rest energy differ by the γ-factor and these two energies are known, the γ-factor can be determined with Eq. 2 [18, p. 20], [23, p. 36].

$$\gamma = \frac{E_{tot}}{E_0} \tag{2}$$

Using the proton mass $m_0 = 1.672\,62 \times 10^{-27}\,\mathrm{kg}$, the speed of light $c = 299\,792\,458\,\mathrm{m\,s^{-1}}$ [18, p. 950] and a total proton energy of $E_{tot} = 7\,\mathrm{TeV}$ corresponding to the proton energy after Run 3 of the LHC we get $\gamma = 7460$.

To understand the behavior of particle beams their dynamics are studied in phase space [18, p. 213ff.], [23, p. 88ff.]. Three subspaces can be defined, two transverse to the beam direction (usually called $x - x'$ and $y - y'$) and one longitudinal to it (usually called $z - z'$ or $s - s'$). Using the phase space is a helpful tool as due to Liouville's Theorem the occupied volume of the phase space is conserved under certain conditions [18, p. 215], [23, p. 91f.]. The transverse region of the phase space occupied by the particle ensemble of the beam (divided by π) is called the beam emittance ϵ. Given that the emittance is conserved as a consequence of Liouville's Theorem, during its trajectory a particle beam can only change its space and momenta coordinates within the constraint of leaving the emittance invariant. In addition to the unnormalized emittance, the normalized emittance ϵ_n [18, p. 218] can be defined by (Eq. 3)

$$\epsilon_n = \beta\gamma\epsilon \tag{3}$$

with γ being the Lorentz factor (see Eq. 2) and $\beta = v/c$ the relativistic particle velocity.

The emittance can be described by an ellipse in phase space with elliptical parameters α, β, γ which can be observed in Figure 2. The area of this ellipse will be $A = \pi\epsilon$.

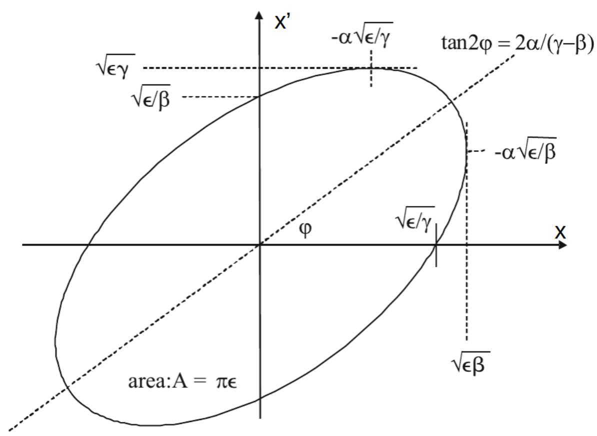

Figure 2: The phase space ellipse and its parameters, taken from [18, p. 219]

As ϵ is invariant, to understand the dynamics of the beam the transformation of the ellipse parameters α, β, γ has to be studied. The particles will always stay on the ellipse, its form however may change. That means, the ellipse parameters are functions of z: $\alpha(z), \beta(z), \gamma(z)$. The $\beta(z)$-function determines the beam size in the spatial coordinate and changes depending on how focused the beam is, that means it has a strong relation to the quadrupole structure [18,

p. 230]. The spatial size of the beam $\sigma(z)$ at a specific longitudinal coordinate z is thus defined by Eq. 4.

$$\sigma(z) = \sqrt{\epsilon\beta(z)} \tag{4}$$

The relation given by Eq. 4 can also be understood observing Figure 2. The space defined by $\pm\sigma(z)$ is called the beam envelope. It is important to mention that there are different σ respectively for the x- and y-transverse direction as the $\beta(z)$ can change individually for each the x and y coordinates.

2.2 General overview of the LHC and its beam dump system (LBDS)

The Large Hadron Collider (LHC) accelerates particles (mostly protons and sometimes lead ions) to an energy of 6.5 TeV (7 TeV for Run 3 beginning in 2021 and High Luminosity LHC (HL-LHC) supposed to start in 2026). The protons are packed in bunches with currently an intensity of 1.15×10^{11} protons per bunch. For the upgrade to HL-LHC the intensity will be doubled.

As the LHC is 26.7 km long and the protons travel at almost the speed of light, the revolution time is 89 µs. As there is a particle free region of 3 µs due to the extraction kicker magnet rise time (see below), the maximum length that can be filled with proton bunches is 86 µs. For a bunch spacing of 25 ns there are 3440 theoretically possible bunch slots. Several bunches are grouped to batches of bunches. The spacing for batches of bunches coming form the pre-accelerators Proton Synchrotron (PS) to the Super Proton Synchrotron (SPS) is 200 ns, thus 8 bunch slots, and the spacing for the injection from the SPS to the LHC is 800 ns, thus 32 bunch slots [8]. With these conditions, filling schemes for the LHC are created. The most common schemes are the Standard (STD) filling scheme with trains of 4 times 72 bunches (see Figure 3) and the Batch Compression Merging and Splitting (BCMS) filling scheme with trains of 3 times 48 bunches [8].

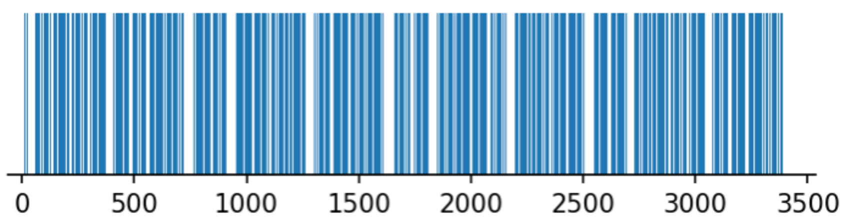

Figure 3: The LHC Standard filling scheme. One line represents one filled bunch position

As the particles circulate at very high energies one main challenge is to hold the hadrons on their circular path. The LHC tunnel is thus equipped with 1232 superconducting dipole magnets each 15 m long [3, p. 161], that is about 70 % of its 27 km. These bend the beams due to the Lorentz force (see Eq. 1) and thus make them stay on a circle.

Fast magnetic kickers are used for the extraction and dilution of the LHC beam. The LHC beam dump system, located in point 6 of the LHC, works as follows (for an overview see Figure 4):

When a beam dump is executed, the beam first gets extracted horizontally from its regular path with 15 fast-pulsed Ejection Dump Kicker magnets (MKD). These magnets have a rise time of 3 µs. Hence in the LHC there is always a particle free region with a duration of 3 µs called the abort gap. The triggering of the MKD thus has to be synchronous with the abort gap with the aim that its field can rise without affecting the particles in the beam.

If this is not the case, some particles get a kick while the field is rising thereby getting deflected less than needed to reach the beam dump line. Therefore, dedicated diluter blocks are installed

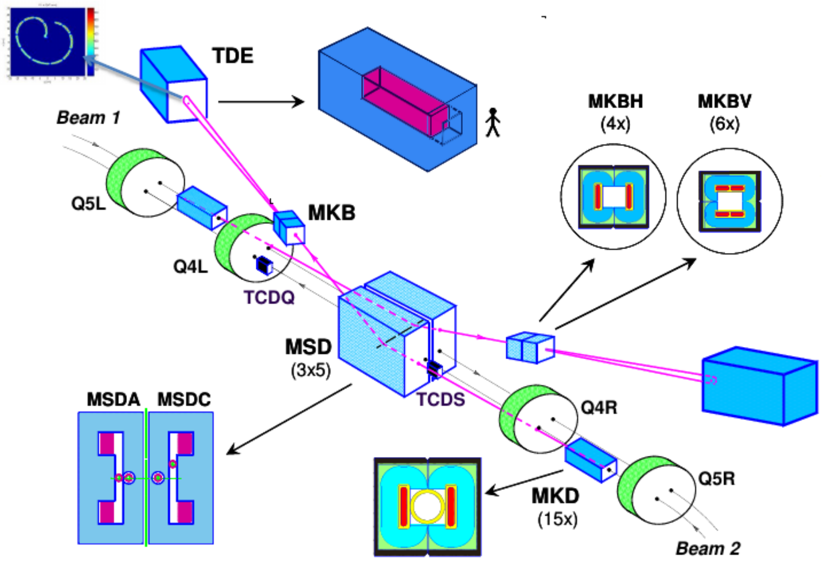

Figure 4: Overview of the LHC beam dump system (LBDS), taken from [2]

in front of the septa magnets (TCDS) and the downstream quadrupole (TCDQ). Such an event is called an asynchronous beam dump.

After the MKD rise-time and during the time the beam gets extracted the MKD kickers have two field overshoots of 5.4 % at flat top (i. e. maximal) energy so their deflection is not constant during beam extraction. These overshoots affect the dilution pattern as explained in 4.1.1 and 4.1.2. The maximum system kick angle at the overshoots of all 15 MKD is 0.286 mrad.

The beam that was successfully kicked out of its normal path in the next step travels off-center through a horizontally defocusing quadrupole (Q4) getting an additional horizontal kick of 30 %. The total horizontal deflection due to the MKD and the Q4 is thus 0.372 mrad.

After the horizontal deflection by the MKD and the Q4 the beam gets vertically deflected by 15 septa magnets [3, p. 441]. These magnets have a high-field region (giving the particles that travel through this part a deflection) close to a field free region (leaving particles travelling through that part on their original path) separated by a thin septum. The kick given by the septa magnets raises the beam above the LHC machine cryostat [3, p. 441]. This kick will not be analyzed in this work.

When the beam is already in the dump line, approximately 100 m downstream of the septum magnets [25, p. 1], it passes through the Diluter Dump Kickers (MKB). First, there are 4 horizontal kickers MKBH (with a maximum kick angle of the system of 0.271 mrad) and then 6 vertical kickers MKBV (with a maximum kick angle of the system of 0.272 mrad). Two MKB of the same type are installed together in one vacuum tank. After the extraction and dilution (see 2.3) the beam is directed towards the beam dump block (Target Dumps External (TDE)). The total drift length between the first extraction kickers MKD and the dump are 976 m [19].

The core of the dump block is constructed of several graphite layers with a total length of approximately 8.4 m and a diameter of 0.7 m and is kept in a nitrogen atmosphere at an overpressure of 200 mbar [25], [10], [12]. Graphite was chosen as a material because of its high melting point [3]. High-energy particles that interact with matter lead to particle cascades [25]. The dump core has, first, graphite layers with a high density to expand and distribute these particle showers, then layers with a lower density to ensure a drift and is ended with other layers of higher density to ultimately slow down the particle showers. The core is separated from the vacuum of the beam dump line by a carbon-carbon composite and a stainless steel foil, this is called the upstream (US) window [11], [22]. At the end of the core this is separated from the atmosphere by a titanium plate, the downstream (DS) window [12]. The US window is directly exposed to the primary protons, that means the energy deposition here is very localized. Whereas the energy deposition in the dump core and the DS window is determined by the smearing out of the dilution pattern due to particle showers.

The dump block is surrounded by a radiation shielding of around 1000 t of concrete and steel [12].

2.3 The dilution system and failure cases

The purpose of the dilution system is to reduce the energy density at the beam dump block. Therefore, horizontal and vertical dilution kicker magnets sweep the beam over the front surface of the dump [25, p. 1]. Figure 5 shows the kick angle that is proportional to the magnetic field of the extraction (MKD) and dilution (MKB) kickers. The beam thus gets swept over the dump in a form close to a spiral (for a detailed description of the creation of the dilution pattern see 4.1.1).

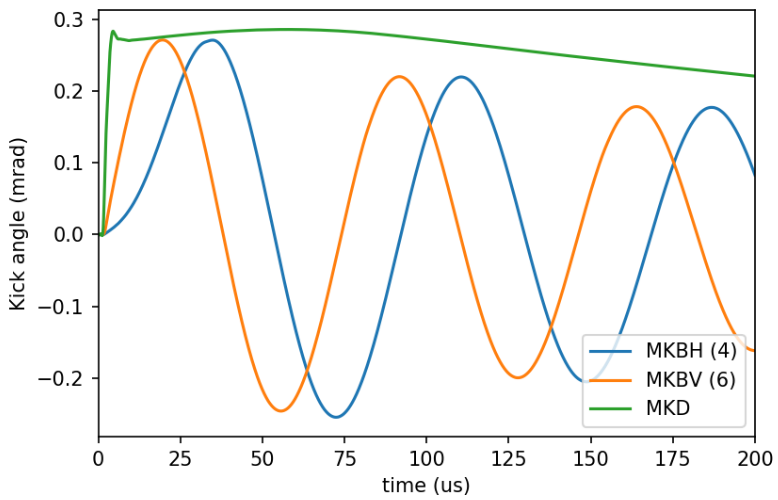

Figure 5: The extraction and dilution kicker waveforms[1]

There are two main failure cases for the dilution kickers that can occur during a beam dump: A flashover can occur in the magnet tank leading to loss of the dilution provided by this magnet and a kicker can get triggered erratically leading to the risk that this kicker is in counter phase to the remaining kickers.

A flashover in the magnet tanks means that there is an arc-discharge with the current going through a plasma generated between the busbars of the magnet coils. If the current does not go through the magnet coils this magnet's field is lost. As there are always two magnets installed together in one vacuum tank, a flashover at one magnet can also propagate to the second magnet. Losing two horizontal kickers is considered to be the worst dilution case that still has to be acceptable for the dump [20].

On July 14th 2018 for the first time during LHC beam operation, a flashover of two MKB happened losing two kickers in the vertical plane. As the flashover for the second magnet happened at a point where there was already current in the coils, the field of this magnet was not completely lost having the effect that for specific times during beam extraction it worked against the rest of the vertical dilution kickers. That meant that in the end the dilution was less

[1]In this plot and in all other plots "us" means "µs"

than if two magnets had just not worked. In this case it happened in the vertical plane, but if a similar flashover happened at the horizontal kickers this would lead to a new worst case (for closer studies about this new failure case see [19]). However, studying this new failure case is not part of this work and so here we assume as worst case the loss of two MKBH kickers.

The second important failure case is the erratic prefiring of a dilution kicker. If a magnet generator gets triggered before the others start working, its waveform (see Figure 5), depending on the time difference to the other generators, might be in counter phase with the other kickers. If the waveforms and thus the kick angles are in counter phase, this leads to a decrease of dilution in that plane. At the end of 2016 it was discovered that there is a possibility that more than one kicker prefires. As mitigation, it was decided to implement an MKB retrigger system from Run 3 on [20], [22]. That means if one dilution kicker is triggered erratically, all the other kickers are triggered as well. As then all the dilution kickers are fired a beam dump has to be executed to avoid having a circulating beam while the dilution system is already working. That means, as for every extraction, the extraction kickers MKD have to be fired. But in order to avoid an asynchronous beam dump one has to wait until the abort gap reaches the position of the MKD before they are fired. That means, the MKD are not fired simultaneously with the MKB but a time delay between the two kicker types is introduced due to the waiting for the abort gap. As the revolution time of the LHC beam, including the abort gap, is 89 µs, the duration of this time delay can be anything between 0 µs and 89 µs. Given that the beam will then get extracted when the dilution kicker waveforms are at a different point as in a nominal beam dump, this will lead to a change in the dilution pattern which in turn can lead to a change in the maximum energy deposition (for the changes in the sweep pattern and the effect on the energy deposition see 4.1.2). As the MKB retrigger system will be implemented from Run 3 on it is important to study its implications for the beam dump [19]. In this work the terms “retrigger time” and “delay time” will be used as synonyms. The retrigger patterns for time delays between 0 µs and 35 µs are shown in Figure 6.

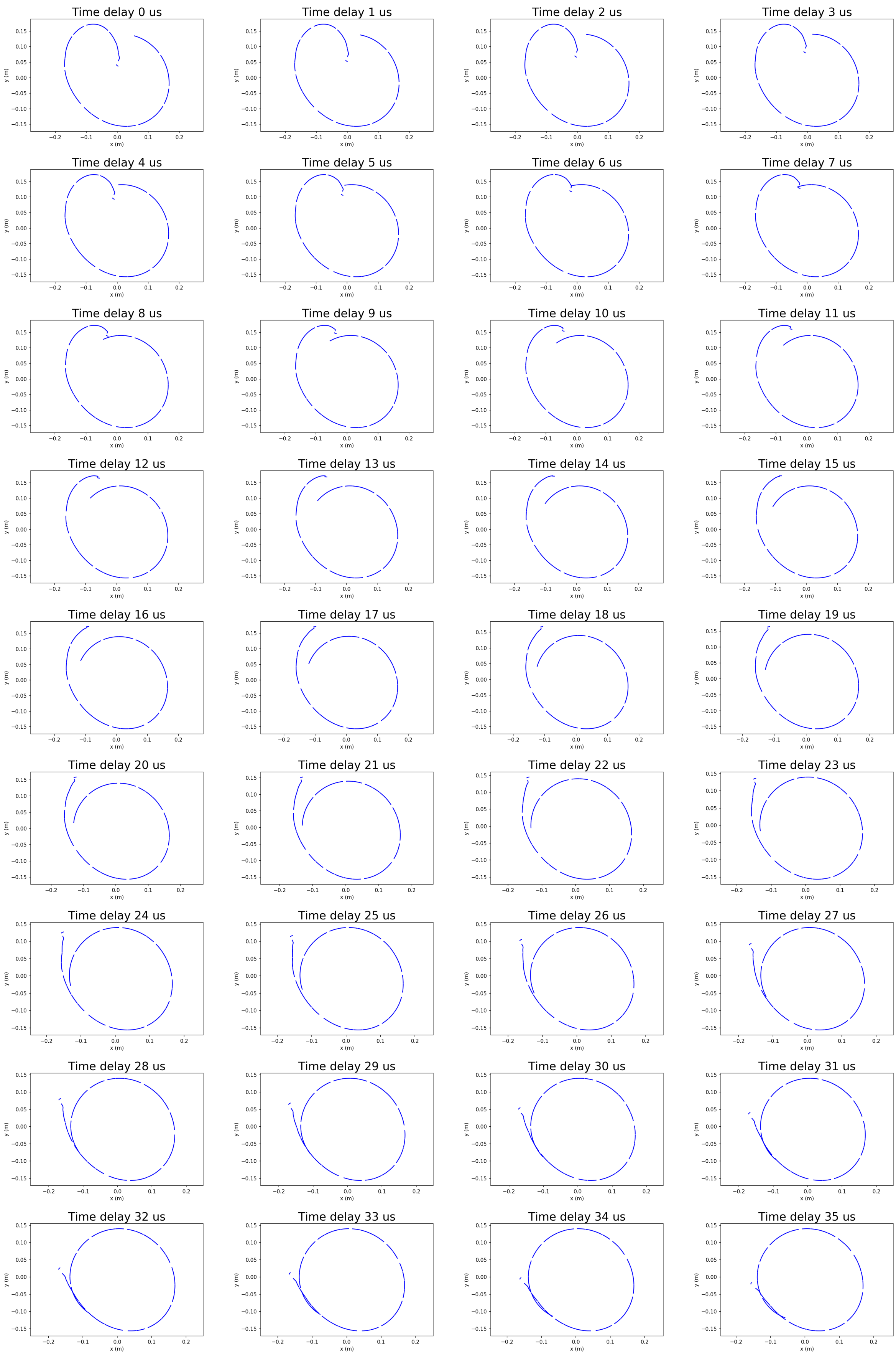

Figure 6: Retrigger patterns with current MKBH waveforms for delay times between 0 µs and 35 µs

3 Method: Python-routine for modelling the beam dilution

3.1 General remarks on the code

Within this thesis an efficient Python routine was written to quickly estimate the impact of different dilution kicker waveforms to the dilution pattern and estimate the density of the patterns.

An existing routine [22] using beam transfer code (MAD-X) is used for benchmarking (see 3.2). The beam transfer code simulates the path of the beam through the whole LHC ring and in the dump lines. All relevant beam dynamic parameters (see 2.1) are taken into account. Some values given by this routine are used for the new Python routine. It is referenced here as "MAD-X Twiss file" [21].

The newly developed Python routine uses a simple model for the dilution: For each type of magnet the kicker waveforms were summed up to have only one integrated waveform for the MKD, MKBH and MKBV respectively. This can be done because for all the kickers of one type the drift length is approximately the same. This is also why in a next step for each type of magnet only one effective drift length is used. For each type of magnet the drift lengths of the first and last magnets are taken from the MAD-X Twiss file and the average drift length is calculated. This average drift length is then used as the effective drift length for each type of magnet. The use of these effective drift lengths means a maximal error of 1.4 % for the MKD, of 0.7 % for the MKBH and of 0.9 % for the MKBV. The maximal error occurs for the extreme kickers. The closer the kickers are to the middle of one kicker series the lower is the error for their drift length. The values for the effective drift lengths are shown in Table 1.

MKD	MKBH	MKBV
950.91 m	646.22 m	635.08 m

Table 1: *Effective drift lengths for each type of magnet until the dump used for the calculation of the dilution sweep patterns*

The procedure of the script is as follows: In the beginning all needed data is loaded. This includes measured waveforms, data for the LHC filling schemes and data from energy deposition simulations. In the next part used parameters are defined. An important parameter to mention here is the time when bucket 1, that is the first slot, that could be occupied with a bunch, is extracted. The abort gap (see 2.2) is 3 µs long. But bucket 1 might not be placed directly after the abort gap. The exact length of the particle free region can thus be set here. Also the beam length can be chosen here.

The measured magnet data is filtered to reduce noise effects. Furthermore, the data is interpolated to have a data point every 5 ns, which is needed for later analysis.

Another important part of the code is the fitting of the data of the MKB waveforms. This is done so that later the attenuation of the damped sine can be changed. One challenge for the fitting is that the MKBH waveforms do not start directly as a damped sine but have a slower rising ascent (see Figure 5). So this first part (the first 24 µs) are fitted with a quadratic fit and the rest with a damped sine. Because of this piece-wise fit there is a slight discontinuity in the fitted curve at 24 µs but this does not have major impacts on the analysis. A function is then written using the fitted parameters and with the damping factor as an argument so that waveforms with different attenuation can be created. In this function the first maximum is rescaled so that the maximum kick angle stays always the same. In contrast, the MKBV waveforms can directly be fitted with a damped sine.

At the heart of the code are two functions. The first function is used when a dilution pattern is already given and has to be analyzed. This function takes as arguments the x and y coordinates of the pattern, the time and a Boolean variable to define whether a possible overlap in the beam sweep path (see 4.1.2) should be calculated or not. The function then calculates and returns the particle velocities in the horizontal, vertical and radial directions, the particle densities along the pattern as well as the maximum density and if required a possible overlap. Using this function in a loop, several patterns can be loaded and a text file is created including the maximum densities, times for the maximum densities and whether an overlap occurs. For simplicity for the future user, a separate script is written which calls this function and returns the mentioned text file for the loaded patterns.

The second function is used when MKD and MKB kicker waveforms are given and the dilution patterns have to be calculated first before they can be analyzed. This function takes as arguments the maximal delay time between MKD and MKB (here often to referred as "retrigger time") in µs (see 4.2.3), the integrated data for the MKD, MKBH and MKBV waveforms, the number of active MKBH and MKBV, the used LHC filling scheme and the possibility to switch the calculation of the density and the overlap off or on for each of the three dump locations: US window, dump core and DS window, with Boolean variables. First, the function calculates all patterns for all retrigger times. It then applies the selected LHC filling scheme and calculates the density along the pattern, the maximal density, the velocities and the possible overlaps. All these values are returned for the selected filling scheme as well as for the theoretical case that every bunch slot in the LHC is occupied, that is one bunch every 25 ns.

Following these functions there are routines to plot the retrigger patterns, the particle velocities, the density distribution along the pattern and the maximum densities for all retrigger times in comparison with simulations for the energy deposition (see 3.2.2).

3.2 Benchmarking

3.2.1 Benchmarking the dilution pattern

The dilution patterns[2] are calculated in the following way: In the beginning of the script the indices for the start and end of the beam (in µs) are defined. The arrays that include the interpolated kick angles for the MKD, MKBH and MKBV are then sliced according to this beam length. Furthermore, only every fifth data point is taken as every 25 ns there is a possible slot for a proton bunch. For the retrigger scenario while calculating the different patterns a loop index is added so that the MKB kick angle arrays can be sliced according to the corresponding delay time. The total horizontal and vertical dilution for each retrigger pattern is then calculated as follows:

$$\begin{aligned}
\boldsymbol{horizontal_dilution_array} &= -\,(number_active_MKBH \times MKBH_drift \\
&\quad \times MKBH_waveform_sliced_for_retriggering \\
&\quad + MKD_waveform \times MKD_drift \times strength_quadrupole) \\
&\quad + horizontal_shift \\
\boldsymbol{vertical_dilution_array} &= \quad number_active_MKBV \times MKBV_drift \\
&\quad \times MKBV_waveform_sliced_for_retriggering
\end{aligned}$$

That means the sliced arrays for the MKB are multiplied by the previously defined drift lengths (see Table 1) and by the number of active MKB (it has to be given in fractions of 4 and 6 respectively). The sliced array for the MKD is multiplied by the MKD drift length and by a factor for the additional kick of 30 % that gives the quadrupole (see 2.1 and 2.2). For the dilution in the horizontal direction the products including the MKBH and the MKD are then added and a minus sign is set in the beginning of the term as the positive parts of the MKBH waveforms move the beam in the negative x-direction using a coordinate system that follows the beam (negative x-direction means to the left from the center of the beam dump line) which is

[2]For a detailed explanation of the creation of the dilution pattern see 4.1.1

how the dilution pattern is usually displayed. For the dilution in the vertical direction only the product of the MKBV array, drift length and number of active MKBV is needed.

The nominal dilution pattern, that is how the beam sweep path looks like on the front-face of the dump for a normal beam dump, is benchmarked for the current waveforms with the nominal pattern calculated with the MAD-X beam transfer code using the same filling scheme that is the Standard filling scheme for beam 2. For this several parameters are adjusted: An important factor is the length before bucket 1 including the abort gap. The assumed length for the MAD-X calculations was 3.9 µs so in the new script the length of the particle free region before the beam starts is also set to 3.9 µs. Another parameter is the horizontal shift. The MAD-X routine uses a coordinate system with its (0,0) coordinates in x and y in the center of the beam dump line. As in the Python routine the deflection of the MKD and the Q4 is summed to the deflection of the MKBH, there is a horizontal offset with respect to the center of the beam dump line of 0.354 m (using the maximum kick angle of MKD+Q4 times the MKD drift length). This offset is corrected by shifting the pattern 0.354 m in the positive direction. This is achieved by summing this horizontal shift to the term of horizontal dilution.

For comparison the pattern calculated with the new Python routine is plotted together with the pattern calculated with beam transfer code and thus showing the result of the benchmark (see Figure 7).

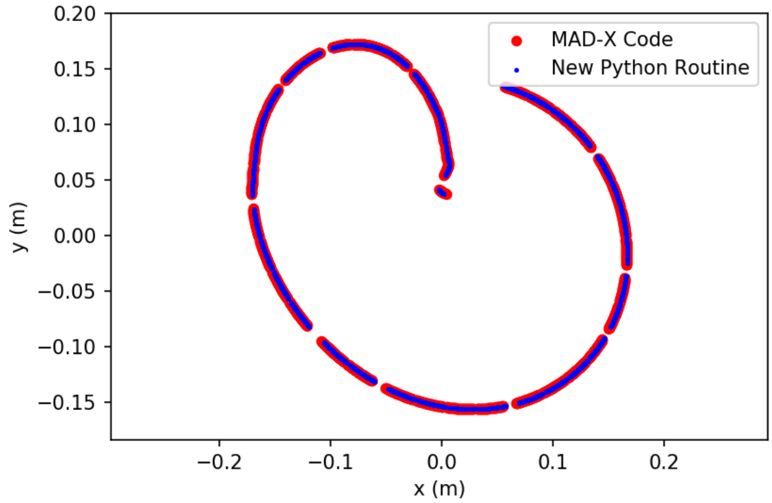

Figure 7: Benchmarking of calculated pattern with new Python code to existing beam transfer code using MAD-X.

The benchmarked pattern fits to the one calculated with beam transfer code. The average difference of the bunch positions calculating the pattern with the two manners is 1.4 mm. It is assumed that the new routine works well for the calculation of patterns and returns reliable results.

The accuracy of the benchmarking is further confirmed by comparing several retrigger patterns calculated with the new routine together with the ones calculated with the MAD-X beam transfer code (see Figure 29, Appendix).

3.2.2 Benchmarking the proton bunch density

The energy deposition for a given dilution pattern at the US window, the dump core (TDE) and the DS window was estimated using FLUKA that is based on Monte-Carlo simulations [7]. In the end what is crucial are the thermo-mechanical stresses because if they get too high there is a risk for damage and thus for the integrity of the system [4], [25], [6], [24]. For studying the thermo-mechanical stresses, dedicated simulations are required which are not part of this work. The energy deposition is related to the stresses [10], [12] and is thus a first indicator of which scenarios are critical.

One goal of this new Python routine is to get a fast estimate of the energy deposition using the density of bunch centers[3]. The assumption for this idea is that the energy deposition is correlated to the density of bunches in the pattern.

The approach in the code is as follows: For each data point, which represents one bunch, the number of bunches within a certain distance is counted. Figure 8 gives a qualitative explanation of the method. The density is calculated for every bunch of the pattern and then the point with

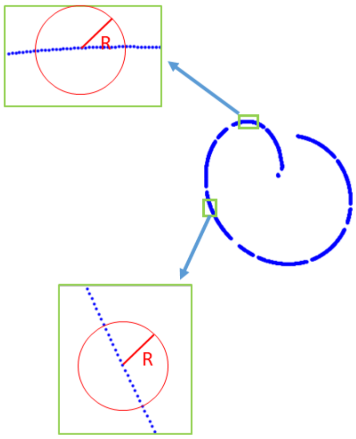

Figure 8: A qualitative explanation of the method to estimate the bunch density

the highest density is taken as peak density for each pattern. Also in the analysis of the FLUKA data the peak value of energy deposition of each pattern is always used.

The energy deposition at the US window is related mostly to the direct impact of the proton bunches at the stainless steel window. That is, as here the bunches are not penetrating a lot into material where they will deposit energy it is assumed that broadening due to particle shower development does not play an important role and the energy deposition is thus very localized. For that reason the radius that should be used to give an estimation of the energy deposition at the US window is assumed to be on the scale of the beam size.

In contrast to what happens at the US window, during its energy deposition in the dump core and even more at the DS window the beam is penetrating a lot of material. So in these cases particle showers play an important role for energy deposition. The particle showers cause the density to be smeared out, meaning that the energy deposition is not localized but will include a wider region as the showers of neighbouring bunches will overlap. That means for estimating the energy deposition at the dump core the distance within which the bunch centers are counted should be much bigger, probably several beam sizes, and the distance representing the estimation for the DS window should be the largest.

The procedure of the benchmarking is as follows: The patterns and corresponding energy deposition were simulated for the current MKBH, MKBV and MKD waveforms for the HL-LHC Standard filling scheme and HL-LHC parameters (that is $\epsilon = 2.08\,\mu\text{m}\,\text{rad}$, bunch intensity $N_p = 2.3 \times 10^{11}$ and an energy of 7 TeV for each proton) with MAD-X and FLUKA for the retrigger scenario until a time delay of 150 µs [7]. That means there is an estimation of the energy deposition for 150 different patterns for the three locations. These same waveforms

[3] For this analysis one proton bunch is represented by one data point. This is why we use here the terms "bunch" and "bunch center" as synonyms. The intensity of the bunches, that is the number of protons in each bunch, is not taken into account

and the same filling scheme are used to benchmark which radii should be used to calculate the density at the US window, the dump core and the DS window. For this, first, all the peak densities are calculated for different circle sizes with radii between 0.1 mm and 41 mm (increasing by 0.1 mm between 0.1 mm and 1 mm, and by 1 mm between 1 mm and 41 mm) for all the 150 retrigger times. These peak densities are then normalized to the density of the nominal pattern and plotted together with the normalized FLUKA data. By observing these plots it is checked which distances seem to best fit the FLUKA data. After getting a general idea of how the density estimation changes with the radius, a range of radii is identified for each location (between 0.5 mm and 2.4 mm for the US window, between 14 mm and 17.4 mm for the dump core and between 18.5 mm and 20.9 mm for the DS window). The peak densities for all retrigger times are calculated for radii within these three ranges with a step of 0.1 mm. To choose which of these density calculations best fits the corresponding FLUKA simulation, for each calculation the normalized peak densities are plotted together with the normalized FLUKA data and the absolute difference between these two curves is calculated. It turns out that the density calculation is quite sensitive when using small radii (as in the range for the US window) but does not change a lot when using bigger radii (as the ranges for the dump core and the DS window). Finally, by minimizing the absolute distances with the FLUKA data and also by cross-checking the plots, a radius is identified for which the density calculation best fits the FLUKA calculation of the energy estimation for each of the three dump locations. These radii are shown in Table 2. The result of the benchmarking is shown in Figure 9.

It can be observed that especially for the DS window the new routine underestimates the parts with low energy deposition whereas it overestimates the peaks. Also the peak around 5 µs for the US window is overestimated. It can thus be concluded that this new approach leads generally to rather conservative conclusions overestimating in some cases the problematic patterns.

US Window	Dump Core	DS Window
1.8 mm	14.6 mm	19.9 mm
$1.4\sigma_x$	$11.3\sigma_x$	$15.4\sigma_x$
$1.6\sigma_y$	$12.7\sigma_y$	$17.3\sigma_y$

Table 2: *Radii used for the density calculation representing the energy deposition and the number of σ of beam size that are lying in these radii*

The beam size at the beginning of the dump block is $\sigma_x = 1.3$ mm and $\sigma_y = 1.15$ mm (calculated with Eq. 3,4,2 using $\beta_x = 5011.2$ m, $\beta_y = 3953.9$ m [21] and $\epsilon_n = 2.5$ µm which is the design emittance for HL-LHC [1, p. 7]). Table 2 shows how many σ lie within the corresponding radii.

One important result of this work is that this simple model of counting bunch centers within a certain region can be used to estimate the energy deposition based on a previous benchmark against FLUKA simulations.

As the bunches are here counted within certain distances with a sharp cut we assume an error of 2 bunches as on each side (see Figure 8) one bunch might be cut at the edge of the radii that are used for the density calculation.

After identifying the radii that represent the density at the US window, the dump core and the DS window, these radii are also used to determine whether for a given pattern an overlap occurs in the sweep pattern or not. Observing the retrigger patterns, one can see that if an overlap occurs this means that some part of the first quarter of the pattern overlaps with the last quarter of the pattern. Because of this, for a given pattern two new arrays are created: One including the first quarter and one including the last quarter of the pattern. For these two arrays all the distances between the pattern points are then calculated and if one of these distances is less than the corresponding radius, "1" is assigned to the overlap-output-array indicating that an overlap exists. If no distance between the first quarter and the last quarter is less than the

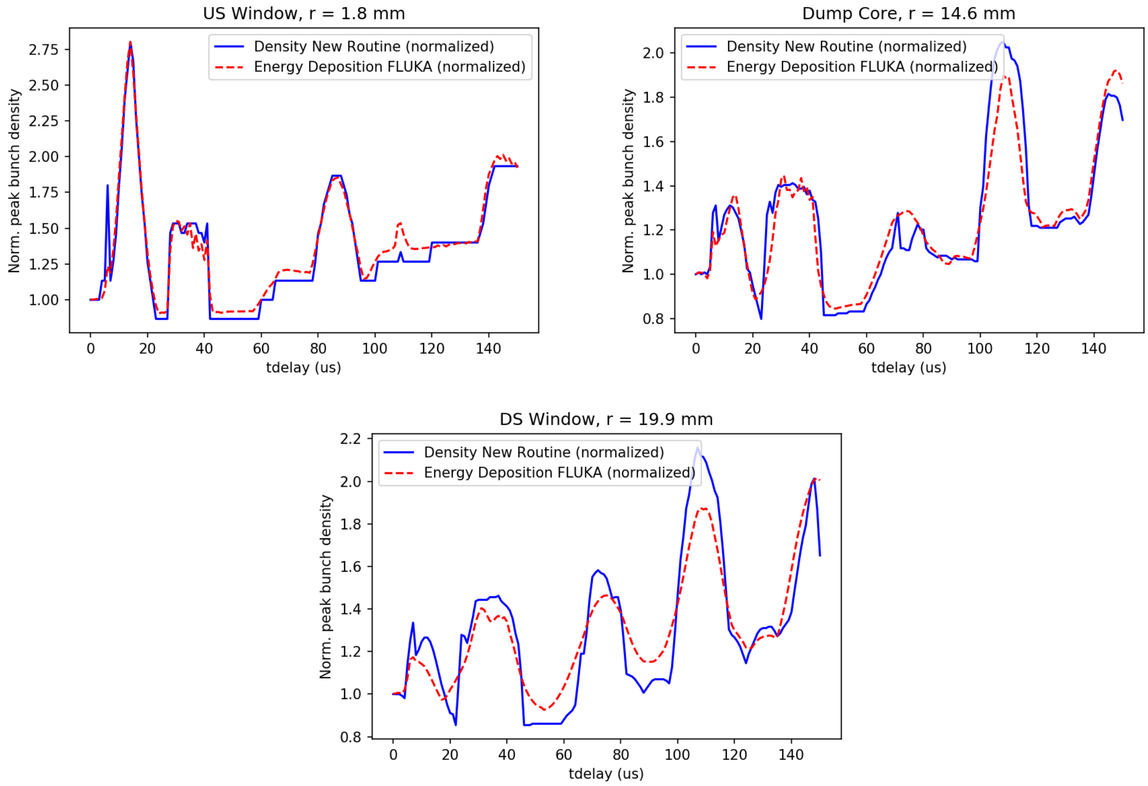

Figure 9: Comparison of the proton bunch density calculation and the energy deposition simulated with FLUKA

corresponding radius, "0" will be assigned to the overlap-output-array indicating no overlap.

That means that the overlap will be calculated for the three dump locations and for each location it will depend on the previously defined radii whether a pattern is considered to have an overlap or not.

4 Studies

4.1 Characterization of the dilution pattern

4.1.1 Analysis of dilution pattern

The shape of the dilution pattern is created by the interaction of the waveforms of three types of magnets: 15 fast-pulsed extraction MKD magnets and 10 fast-pulsed dilution magnets of which 6 MKBV (vertical deflection) and 4 MKBH (horizontal deflection). The waveforms for these magnets (with the integrated deflection angle for each type of magnet) are shown in Figure 5.

The general form of the pattern is close to a spiral (or a cursive e rotated by 90° counter clockwise), see Figure 7. It is created by the two damped sine waveforms of the dilution kickers that are shifted around 90° from one another due to the slower rise of the MKBH. With this, during a nominal extraction the beam first gets deflected mostly vertically while the horizontal kickers rise. At the maximum of the vertical kick angle (15.7 µs after the beginning of the beam extraction, that is when bucket 1 is extracted) the horizontal field rises and starts to dominate the deflection moving the beam to the left from the center in beam direction. The horizontal deflection reaches its first maximum 31.1 µs after the beginning of the beam extraction. Shortly after that, the deflection in the vertical direction passes through zero to then increase in the opposite direction deflecting the beam in the negative y-direction reaching its negative extremum at 51.7 µs. Then the vertical deflection decreases again while the horizontal deflection rises sweeping the beam in the positive x-direction having an extremum at 68.5 µs. In the end both fields rise again but as the sine-like currents are damped, the deflection is less than at the first maximum.

Additionally to the general shape given by the MKB waveforms, the horizontal deflection by the extraction kickers MKD also has an impact on the pattern. The strongest effect is at the beginning due to the first overshoot of the MKD: Instead of being deflected straight to the positive y-direction, the pattern gets an additional deflection in the horizontal direction. It depends on the filling scheme whether or not this extra deflection is noticeable in the nominal pattern: In most filling schemes there are several free bunch positions at the beginning of the pattern. In these cases this extra deflection is hardly visible.

The other effect of the MKD is due to the second overshoot. By the second overshoot we understand that the field of the MKD is not completely constant but has a slight slope with a second maximum even after the first overshoot (see Figure 5). During the first extremum of the MKBH this overshoot gives even more deflection and thus the deflection in the negative x-direction is somewhat increased. During the second extremum of the MKBH, that is in the opposite direction, this overshoot works against the kick of the MKBH and the deflection in the positive x-direction is thus slightly decreased in comparison to what it would be with the MKD field being perfectly constant. So the combination of these two effects shifts the pattern slightly in the negative x-direction.

The vertical deflection is not affected by the MKD as these magnets deflect only in the horizontal direction.

4.1.2 Analysis of bunch density as estimation of energy deposition

The benchmarking (see 3.2.2) shows that the bunch density for specific radii represents well the simulated energy deposition at the different dump locations. In this section, how the density is composed for different patterns shall be analyzed using the current MKBH waveforms.

If there is no overlap in the sweep path, the bunch density is determined by the sweep velocity: If the beam is swept slower, more bunches are deposited close to each other than if the beam is swept fast. So for a pattern without overlap the density at each point of the pattern is proportional to the inverse sweep velocity at that point. This can be observed clearly for the density distribution of the nominal pattern, see Figure 10.

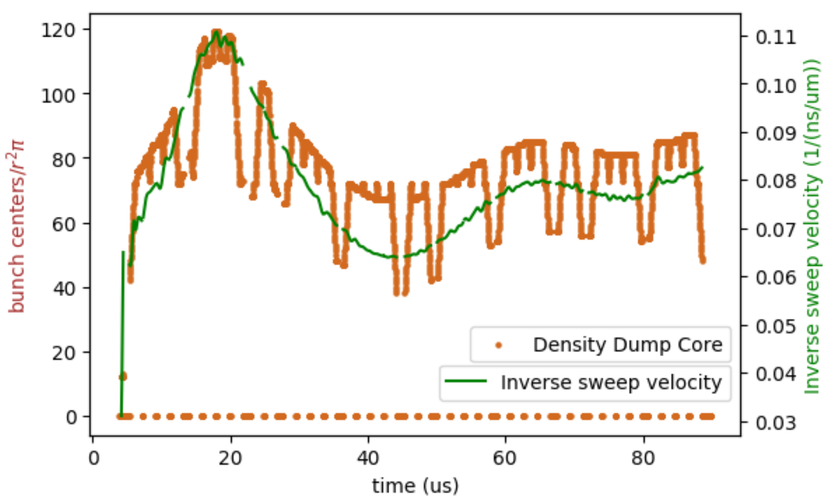

Figure 10: Density distribution in comparison to the inverse sweep velocity along the beam sweep path for the nominal pattern

The structure of the density in Figure 10 is due to the filling scheme: At the end of a bunch train or bunch batch the density will go down (and be equal to zero for gaps free of bunches bigger than the used density estimation radius), as for the bunches close to free slots less bunches will contribute to the density. The decrease of density for long particle free gaps due to injection from the SPS and for short free gaps due to injection from the PS in between can thus clearly be observed.

As the waveforms have the form of a damped sine, the velocity at the end of the sweep path will always be lower than at the beginning. This effect gets even more noticeable for late retrigger times as then the beam gets swept under the impact of much more damping. In particular for late retrigger times there is an elevated probability that the density increases in the end parts of the dilution pattern due to reduced velocity. This is the reason why the density increases for most of the late retrigger times.

Another important issue that reduces the velocity drastically is that for some retrigger times the MKD work against the MKBH during the first overshoot, the so-called Overshoot One. This critical case is explained here by the most important example for that: A delay of 14 µs between the MKD and MKB. Figure 11 shows that the extraction of the first particles after the particle free region occurs at a time when the vertical deflection is almost at its maximum. The bunches thus have almost no vertical velocity at this point and are swept only in the horizontal direction. The first bunches that get extracted are thus moved to the left by the collective action of the

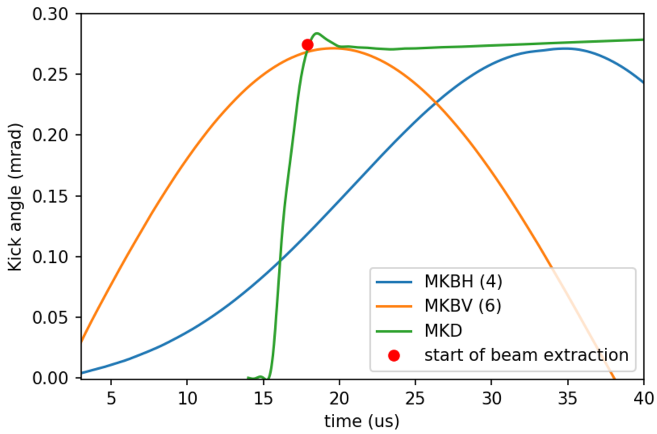

Figure 11: Waveforms at 14 µs retrigger time delay

MKD and MKBH. After their maximum, the MKD switch direction and thus start to work against the MKBH. For a short fraction of time the MKD dominate the deflection moving the beam slightly to the right. But then the MKD and MKBH practically cancel each other out. As there is also hardly any deflection in the vertical plane at this point, the total sweep velocity is close to zero during about 2 µs (see Figure 12). That means all the bunches during these 2 µs hit the dump in a very small region leading to a locally extremely high density. Given that after this short almost-still-standing of the beam it is again swept to the left, the beam goes back and forth three times in a very narrow region. The corresponding pattern with a zoom on the critical region and the distribution of density for this pattern can be observed in Figure 13. The phenomenon of the cancellation between the MKD and MKBH explains the very high peak of density at a delay time of 14 µs in the plot of the densities at the US window for all retrigger times (see for example Figure 9).

After one period of the MKBH, at 86 µs time delay, the same working against of the dilution and extraction kickers happens. But due to the damping the kick angle of the MKBH has already decreased so the sweeping is dominated by the MKD and the deflection is not completely

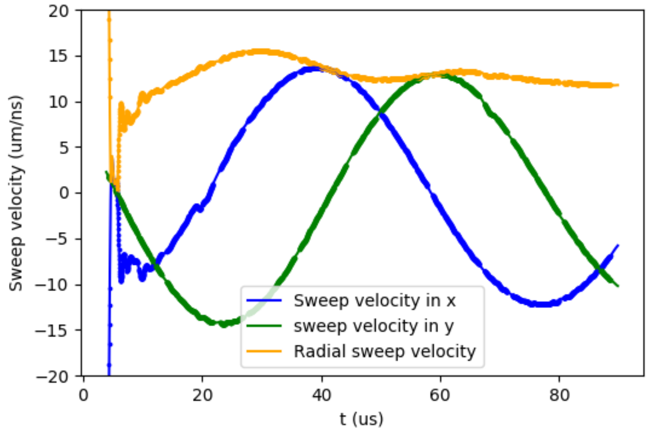

Figure 12: Sweep velocities at 14 µs retrigger time delay. It can be observed that shortly after the beginning of the beam extraction the radial sweep velocity is close to zero.

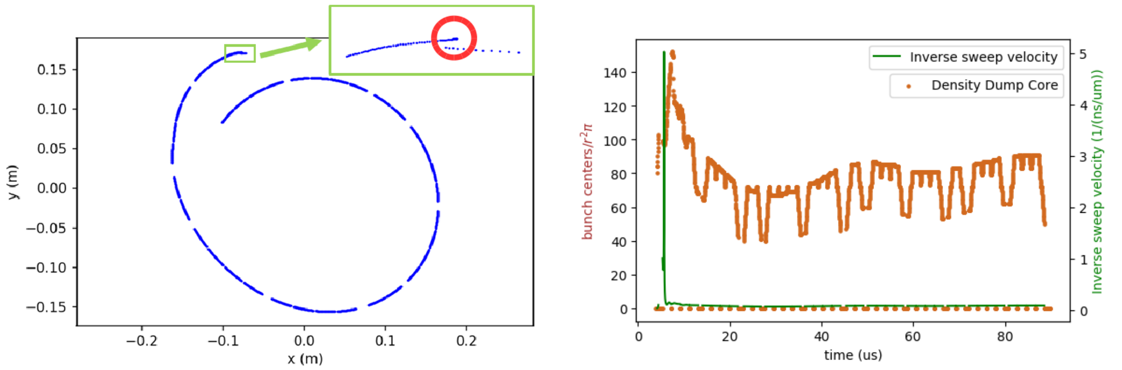

(a) *Dilution pattern* (b) *Density distribution along the beam sweep path*

Figure 13: Extreme density hotspot at 14 µs retrigger time delay due to the working against of the MKD and MKBH

cancelled out as it was at 14 µs where MKD and MKBH kick almost with the same strength. So also for 86 µs time delay an increase in density can be observed but not as strong as at 14 µs.

Half an MKBH period after 14 µs at 51 µs and half a period after 86 µs at 123 µs the extraction and horizontal dilution kickers also work against each other. However, at these times as the MKBH are kicking in the other direction, the beam goes back and forth only twice, whereas at 14 µs and 86 µs the beam goes back and forth three times. Moreover in this part of the beam there are very few bunches for the used Standard filling pattern. This is why no density increases can be observed at the retrigger times at 51 µs and 123 µs. In 4.4.2 it will be explained that for other filling schemes there could be an increase of density for these patterns.

For patterns without overlap in the sweep path the density is determined by the sweep velocity. However, if an overlap occurs, this effect will dominate and lead to very high densities even for points where the beam is swept with a fast velocity. One relevant example for overlaps are the patterns around 34 µs. For these retrigger times the end of the sweep path crosses inside the inner part of the sweep pattern. But as the waveforms do not show a very strong damping, the end of the beam passes almost through the same path. Figure 14 shows this pattern and the corresponding distribution of density.

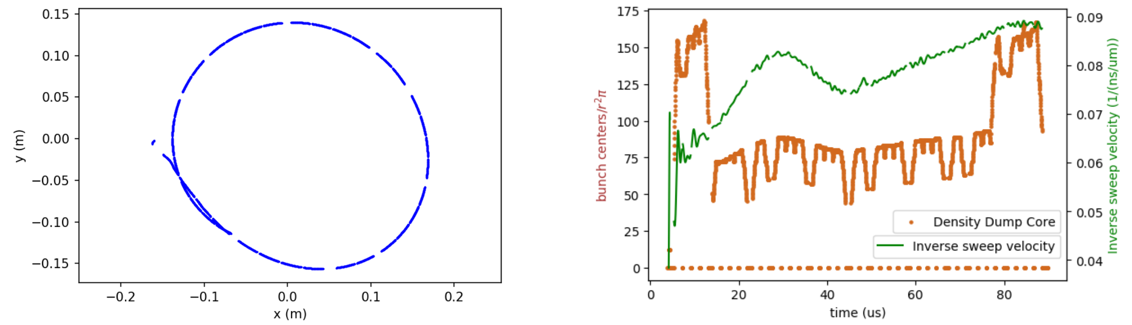

(a) *Dilution pattern* (b) *Density distribution along the beam sweep path*

Figure 14: High density due to overlap for retrigger pattern at 34 µs delay time

It can be observed that for this case the density at the beginning and the end of the sweep path, where the overlap occurs, is not proportional to the inverse sweep velocity so it is clear that in this case the increase of the density is due to the overlap. But still, as the sweep velocity at the end of the beam path is relatively low this increases the density even more.

As stated in chapter 3.2, whether an event is called an overlap or not is defined by the radius corresponding to each dump location that was determined during the benchmarking. For the US window overlaps occur for 6 µs, for 109 µs and around 34 µs, for the dump core and the DS window these overlaps occur at the same retrigger times and additionally around 70 µs.

In summary it can be said that the bunch density is dominated by the sweep velocity for patterns with no overlap, but if an overlap occurs this will determine mainly the maximum density of a pattern.

Figure 15 shows in summary due to which patterns there are density peaks for the retrigger scenario.

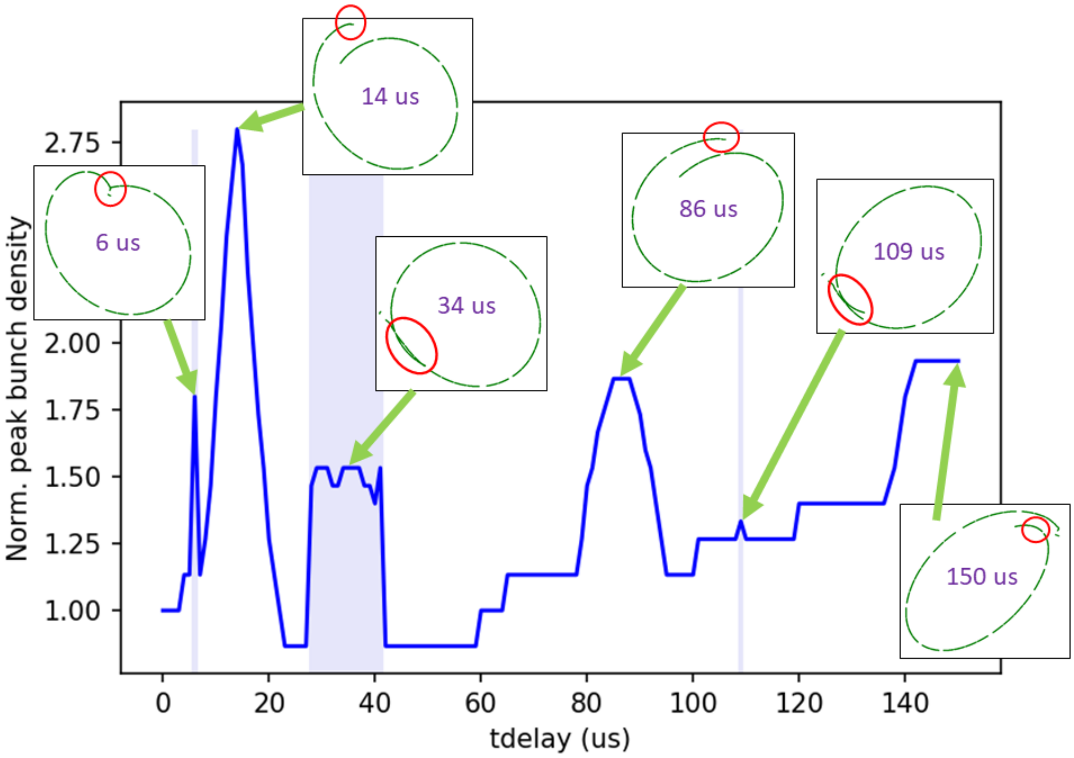

Figure 15: Maximum densities in the US window for all retrigger times and patterns that lead to peak densities. Overlaps occur in the shaded regions

4.2 New MKBH Waveforms

4.2.1 Difference of new MKBH waveforms to current ones

For Run 3 of the LHC, beginning in 2021, the MKBH magnets will be upgraded. The magnets are powered with generators using the discharge of a capacitor. In order to reduce the risk of erratic firing of the generators, their voltage should be lowered. Notwithstanding this change, the current in the magnets has to provide the same kick angle[4]. As the electrical field energy of the generator circuit including the capacitor has to be the same as the magnetic field energy of the inductance (see Eq. 5) all this can be achieved be increasing the capacitance C of the generators [13].

$$\frac{1}{2}CU^2 = \frac{1}{2}LI^2 \tag{5}$$

This change in the generator circuit leads to a slight change in the MKBH waveforms. Since no measurements were available, simulated waveforms [15] have been used for previous analyses [20]. These simulated waveforms show a higher but not constant damping, meaning that there is an attenuation from the first to the second maximum but the next maxima do not get continuously lower. In this work the actual measured new waveforms [14] are analyzed. These measured new waveforms turned out to be more similar to the current ones having less damping than expected by simulations and the damping being constant. Still, the damping is slightly higher than in the current waveforms which is expected to have a small impact on the dilution patterns. The three waveforms can be observed in Figure 16.

The damping of the current waveforms is 81 %, that means the second maximum is 81 % of the first maximum whereas the damping for the measured Run 3 waveforms is 78 %.

[4]The same current according to same beam energy. For 7 TeV beams the current has to be scaled up so that the kick angle stays the same.

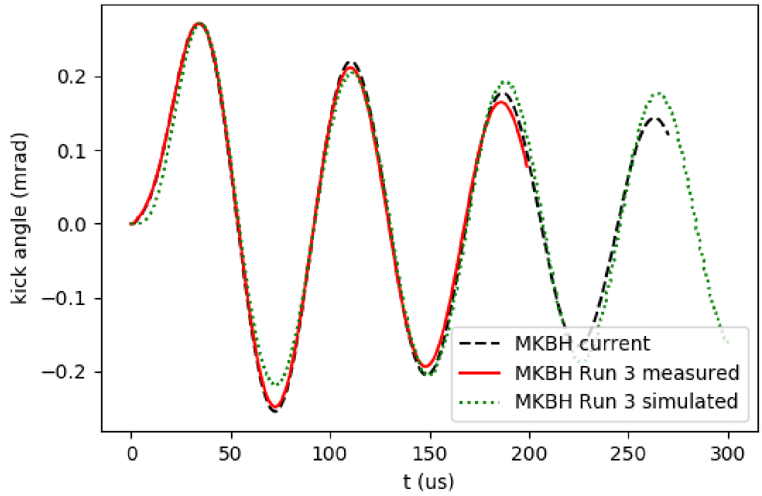

Figure 16: Comparison of current and new MKBH waveforms (measured and simulated), new waveforms measured at 7 TeV, maximum kick angle scaled to current maximum kick angle

The nominal pattern, shown in Figure 17, looks almost the same as with the current MKBH waveforms. Only the positive horizontal deflection is reduced due to the slightly higher damping. The maximum horizontal deflection is 4.1 mm less than with the current waveforms. The densities for the nominal pattern, shown in Table 3, present minor differences. But these differences lie within the assumed error of two bunches and the densities for the nominal pattern can thus be considered to be equal to the ones with the current waveforms. The point for the highest density of the nominal pattern lies for all the three dump locations for the new MKBH waveforms on the same spot. The points of highest density are also in this spot for the current waveforms except for the US window where it is a bit before.

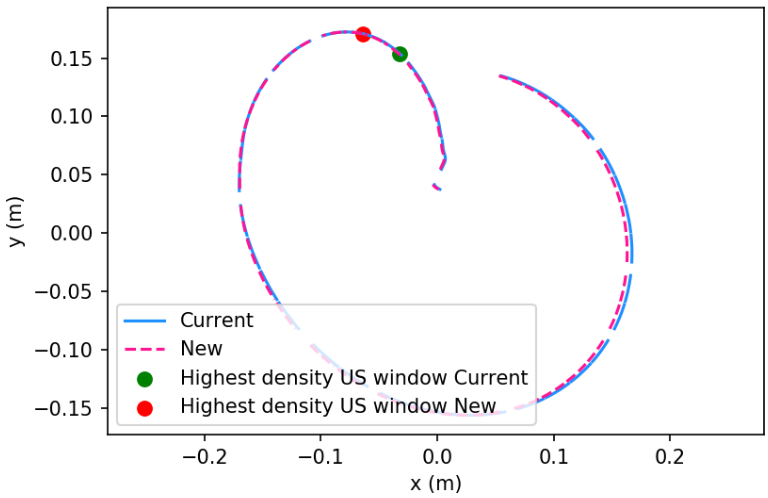

Figure 17: Comparison of nominal dilution pattern for current and new MKBH waveforms

MKBH	US Window	Dump Core	DS Window
Current	15 ±2	119 ±2	158 ±2
New	17 ±2	121 ±2	160 ±2

Table 3: *Comparison of number of bunch centers per πr^2 for the nominal pattern for current and new MKBH waveforms for the LHC STD filling scheme*

4.2.2 Failure case: Missing MKB

Seeing that the new MKBH waveforms do not have a big impact on the nominal pattern, now their impact on the failure cases has to be investigated. We first study the failure case of missing MKB. Here the analysis is done with the BCMS LHC filling scheme as this filling scheme is considered to be more critical for the case of missing MKB. The density calculations are compared with FLUKA data [7] for the energy deposition at the dump core.

The missing of MKB due to a flashover in the magnet tanks (see 2.3) is a prominent failure case so close studies are needed. The change in the dilution pattern for all possibles cases of missing MKB can be seen in Figure 18.

It is assumed that losing kickers in both dilution planes simultaneously will not happen, so only the cases for missing MKB in one plane are considered. For that reason the energy deposition using the new method of bunch densities was studied for missing MKB in one plane. As the available FLUKA data is for energy deposition in the dump core, this was also used here for comparison. Figure 19 shows the increase of density for the current MKBH waveforms, the new MKBH waveforms as well as the FLUKA estimations, everything always normalized to the dilution of the nominal pattern.

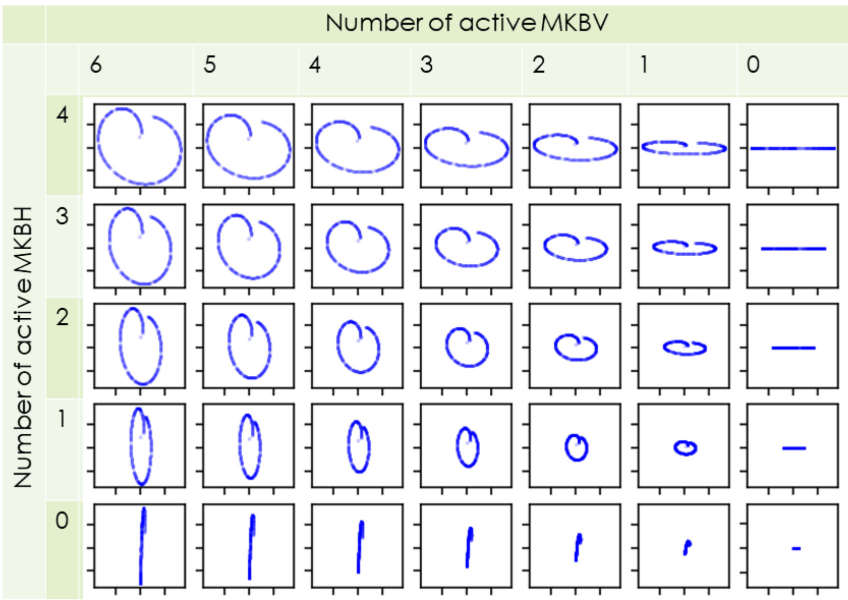

Figure 18: Change in dilution pattern for different number of active MKB

The density increase in percentages of the nominal dilution for all possible cases can be seen in Tables 5 and 6, Appendix.

Figure 19 shows several results: First of all, these curves confirm the benchmarking of the new method of calculating the bunch densities as an approximation of the energy deposition to the FLUKA data: The blue markers, representing the estimation with the current MKBH, fit almost perfectly with the red markers, representing the FLUKA calculations, except if there is no working kicker left. There are therefore two ways that show that this new method gives a

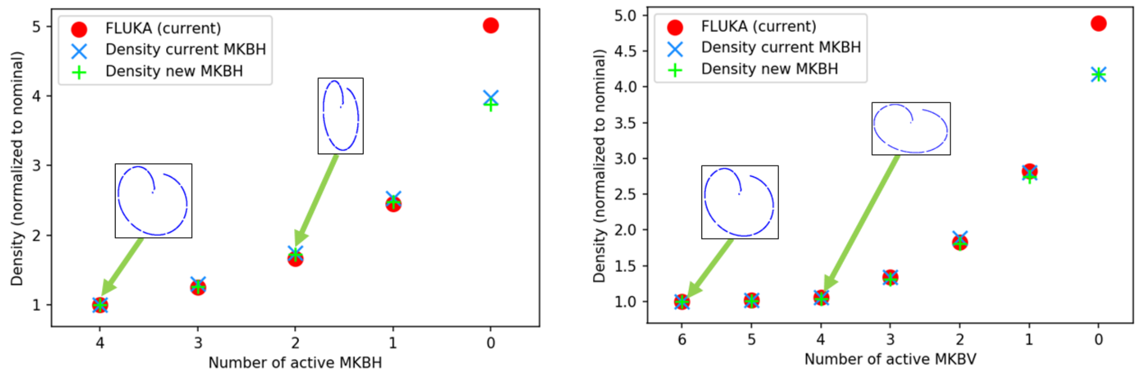

(a) *Missing MKBH* (b) *Missing MKBV*

Figure 19: Increase of estimated proton bunch density for missing dilution kickers in the TDE core compared with energy deposition calculated with FLUKA

good estimation of the energy deposition: The benchmarking for the energy deposition with the retrigger scenario explained in 3.2 as well as Figure 19 for the failure case of missing MKB.

Secondly, the green markers representing the estimation for the new MKBH have in both cases an almost equal behavior to the blue curve representing the estimation using the current MKBH waveforms. That means that for the failure case of missing MKB the density stays the same for current and new waveforms. In most cases the green markers indicate even slightly lower density for the new waveforms but most of the differences are within the assumed error of two bunches.

A third result is the confirmation of what former studies showed [20], [10]: Losing kickers in the horizontal plane is much more critical than losing kickers in the vertical plane. The first reason is that there are 6 MKBV while there are only 4 MKBH, so losing one kicker in the horizontal plane is a much bigger percentage of the total dilution as losing one kicker in the vertical plane. Additionally to that, at the point of highest density there is mostly horizontal dilution. This is why losing 2 out of 4 MKBH is more critical than losing 3 out of 6 MKBV [19]. If there are two kickers missing in the horizontal plane, the total density increases to 173 % (175 % for the current MKBH waveforms) of the nominal one. That means that even if only two out of a total of ten kickers are missing, but these are missing in the horizontal plane, the total density almost doubles. Whereas if we lose two MKBV, the total density is 104 % (106 % for the current MKBH waveforms) of the nominal one, thus not critical.

Additionally to the behavior of the density in the dump core the density in the windows was also studied (see Figures 30 and 31, Appendix). Obviously, in general the density increases for the windows are similar as for the core, if more kickers are lost. The percentage increase on the DS window is almost the same as in the core differing by at most 3 % of the core values if at least two MKB are working (for each plane) but increasing slightly less if fewer than two MKB are working. For the US window the same is true for the new waveforms but not for the current ones. For the current waveforms the density increase in terms of percentages is stronger while losing MKB. If two MKBH are lost, the density already increases to 193 % (171 % for the new waveforms) of the nominal density and if two MKBV are lost it is 113 % (100 % for the new ones) of the nominal density. However, these differences are only noticeable when observing the percentages (always in comparison to the nominal pattern of the respective waveforms). If the absolute values of bunch centers are compared, all differences lie within the error of two bunches. The differences in the percentages are due to the fact that the percentages are given with respect to the nominal dilution pattern of each type of waveform. So in the worst case of losing two kickers in one plane the impact for the dump stays the same with the new waveforms.

4.2.3 Failure case: Erratic firing leading to Retriggering

In case of an erratic firing of more than one MKB generator all the other MKB will be retriggered as well and then the beam will be extracted at the next possibility, that is, when the abort gap is at the extraction kickers to avoid an asynchronous beam dump. The consequence is that the MKB are no longer in phase with the MKD, leading to a change of the sweep pattern (for more details see 2.3). The retrigger scenario is considered to have a delay of at most 96 µs between the MKB and the MKD. All patterns with a delay time of between 0 µs and 96 µs were studied in order to investigate the bunch density at the dump for every possible retrigger scenario.

As the MKBV stay the same for Run 3 of the LHC, no change can be observed in the retrigger patterns in the vertical direction compared with current waveforms. But due to the slightly higher damping of the new MKBH waveforms, there are some small changes in the horizontal direction. That means that in general every extremal horizontal dilution except the one that is due to the first maximum (as the maximum kick angle stays the same) is always a bit less than the extremal horizontal dilution with the current MKBH waveforms. This can be especially observed for retrigger times between 18 µs and 44 µs, between 56 µs and 80 µs and for very late retrigger times of more than 93 µs, as in these cases the end of the beam is driven into the inner part of the sweep pattern (leading to the risk of an overlap). With the new MKBH waveforms the end of the sweep path is significantly further away from the outer part than when observing the patterns with the current MKBH waveforms. In effect, the new MKBH waveforms produce fewer overlaps. One important example is the retrigger pattern of 34 µs (see Figure 20): While using the current MKBH waveforms, the beam crosses the same path twice. Using the new waveforms, however, the beam-end gets very close to the beginning of its path but does not actually cross it.

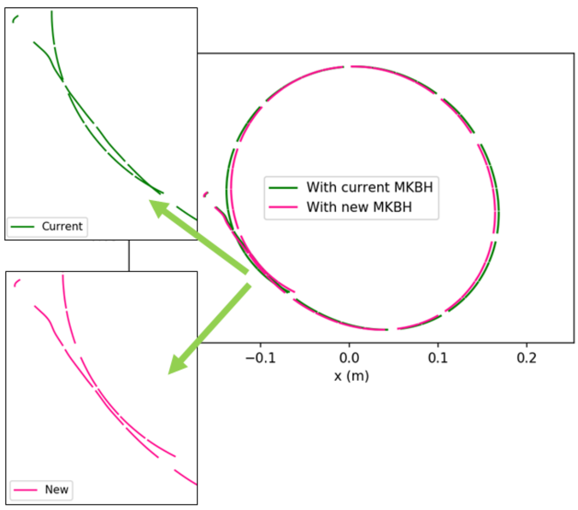

Figure 20: Comparison of a critical overlap pattern at 34 µs delay time for the current and new MKBH waveforms

In total, with the new MKBH waveforms, for the delay times around 34 µs an overlap in the US window only occurs for retrigger times between 35 µs and 38 µs whereas for the current MKBH waveforms for much more retrigger times, namely between 28 µs and 41 µs an overlap occurs.

Another improvement with the new waveforms is the pattern at a delay time of 71 µs and the ones close to this time. At these late retrigger times the end of the beam is swept with relatively low velocity and thus the point of maximum density is often at the end of the sweep pattern. In the patterns around 71 µs, the end is not only slow, but it is also quite close to the beginning of the sweep path. This leads to an overlap in the dump core and in the DS window when the current MKBH waveforms are used. However, using the new waveforms the last part of the beam is swept more inside the pattern due to the higher damping. The slower part of the beam is thus further away from the outer part (that is, the beginning of the sweep path) and no overlap is seen any more for the dump core (see Figure 21 and Figure 22). Even for the DS window a positive development can be mentioned for this pattern: Although the overlap around 71 µs is still seen in the DS window with the new MKBH waveforms, the proton density gets lower as the first and last bunches are further away from each other.

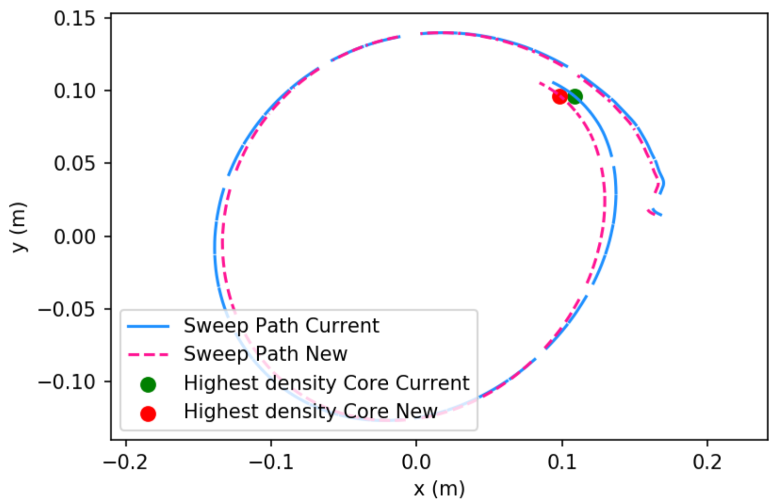

Figure 21: Comparison of the patterns at 71 µs delay time and the points of highest density in the dump core for the current and the new MKBH waveforms

As a next step, the densities for all retrigger patterns are calculated and plotted against the retrigger time delays. Figure 22 shows the maximum density normalized to the respective nominal density for the US window, the dump core and the DS window for all relevant retrigger times for the new MKBH waveforms in comparison to the current ones.

It can be observed that the density in general has a similar behavior for both waveforms. Still, the new waveforms lead to some small advantages especially for the retrigger times mentioned above.

In conclusion, Figure 22 shows that the overlaps get reduced for the new MKBH waveforms in every dump location. More importantly, no new overlaps are created.

As the case of losing two MKBH kickers is assumed to be the worst case, for all the three dump locations the density for losing two MKBH is also plotted for comparison. At the US window, for all retrigger times except the ones around 14 µs the density is lower than for the worst case of losing two MKBH. As former studies have already shown [20] that the peak energy deposition increases noticeably for these retrigger times, the mechanical-stresses produced by these patterns were studied in detail and it was concluded that the thermo-mecanical stresses are lower than in the case in which two MKBH are missing [12].

For the dump core and the DS window the density stays clearly below the value for losing two MKBH for all retrigger times.

Table 4 summarizes the worst case retrigger patterns for the current and the new MKBH waveforms.

It can thus be observed that the maximum densities decrease for all dump locations for the new MKBH waveforms.

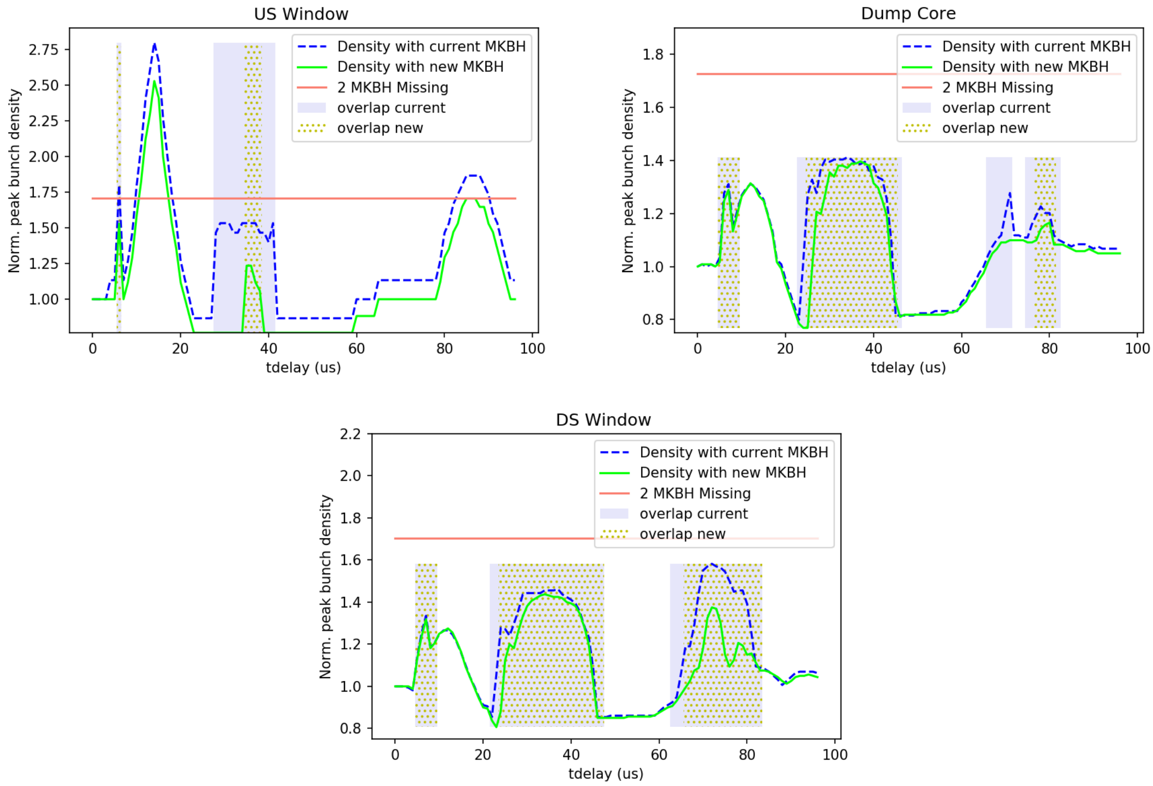

Figure 22: Comparison of the maximum densities and overlaps for the current and the new MKBH waveforms for all retrigger delay times

	Current MKBH waveforms		New MKBH waveforms	
Where	t delay [µs]	% of nominal dilution	t delay [µs]	% of nominal dilution
US Window	14	280	14	253
Dump Core	34	141	37	140
DS Window	72	158	34	144

Table 4: *Worst case densities for the retrigger scenario*

4.2.4 Conclusion

The effect on the dilution patterns and the bunch density was analyzed for the new MKBH waveforms in the nominal case as well as for the failure cases of missing kickers and erratic firing leading to retriggering. The analysis shows the following results:

The nominal pattern stays almost the same with marginally less deflection in the positive x-direction due to slightly higher damping of the new waveforms. In general it can be concluded that the new waveforms do not have a significant impact on the nominal dilution pattern and its energy deposition.

For the failure case of missing dilution kickers the behavior of the new waveforms is, within error bars, the same as for the current waveforms. The analysis of the density confirmed the benchmarking of the density calculations with the FLUKA simulation of the energy deposition.

For the retriggering the new waveforms have a positive effect: The slightly higher damping leads to fewer overlaps and the energy deposition is significantly reduced for several retrigger patterns. For the dump core and the DS window the density stays below the density of the assumed worst case of losing two MKBH in all cases. For the US window the density only exceeds these values for the patterns around 14 µs but the thermo-mecanical stresses were studied for this case and do not exceed the stresses for two MKBH missing.

In summary, the new MKBH waveforms, that should be implemented before Run 3 of the LHC, do not lead to an increment of the density of bunch centers at the dump but are in some retrigger cases even beneficial, leading to a decrease of density.

4.3 Dependence on waveform damping

4.3.1 Motivation and implementation of damping as a variable

The analysis of the new MKBH waveforms showed that a higher damping can reduce the proton density for certain retrigger delay times by reducing overlaps. Therefore, it shall be investigated if a further increase in the damping factor of the waveforms would lead to a further decrease in density. A higher damping would sweep the end part of the beam more inside the pattern as higher damping means less kick angle and thus less deflection away from the center of the dump line. As for certain retrigger delay times the end part of the beam would thus be further away from the beginning of the sweep path, overlaps would be reduced.

The damping of the waveforms can be adapted by a resistor in the RLC-circuit of the magnet generators. Still, this resistance can only be changed in a range of about 1.75 % more or less damping [16] without having to modify the whole design of the generators.

The aim is to investigate whether higher damping could be used to avoid overlaps for the critical patterns in the retrigger scenario. However, a higher damping could also have a negative effect, mostly for late retrigger times: A higher attenuation means that the beam gets less deflected in this plane and thus also has a lower velocity, mainly during the maximum kick angles. This also reduces the radial sweep velocity, which will be more noticeable for larger retrigger delays as the deflection will decrease more strongly and with that the velocity. Having a lower velocity will lead to a higher bunch density. While changing the damping of the waveforms we thus have to make a tradeoff between trying to reduce overlaps and not increasing the density on other retrigger times due to slow sweep velocity.

For the implementation, the MKBH waveforms where fitted as discussed in 3.1. After this fitting, a function is implemented that creates a waveform with the shape of an MKBH with the desired damping. The damping can be set in the percentage of the second maximum to the first maximum. Even if the measured waveforms show a damping of 78 %, due to implementation difficulties for the fitting (see 3.1) of the fitted waveforms the ones with 77 % show the most similar behavior and are taken as a reference. Figure 23 shows the quality of the fit, comparing waveforms, nominal patterns and densities for the retrigger scenario for the measured and fitted waveforms.

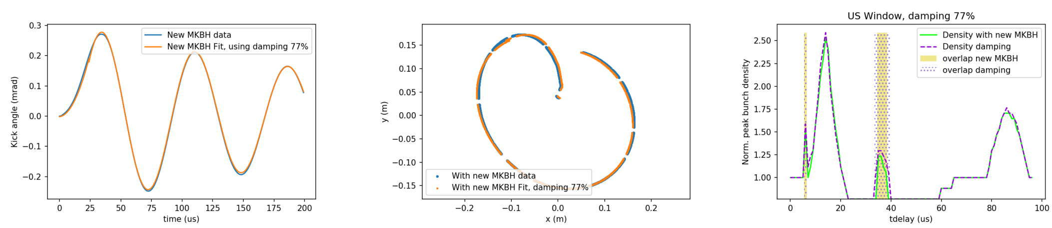

(a) (b) (c)

Figure 23: Showing the quality of the fitted new MKBH waveforms to the measured ones

It can be assumed, that the fit is good enough for the present investigations. The positions of the points of highest density were also checked for the three dump locations and they were found, in the majority of cases, to be in the same part of the sweep pattern for the measured and the fitted waveforms. By observing Figure 23 it can also be seen that the density peak around 5 µs is overestimated using the fit. This has to be borne in mind for further analysis.

Even though the MKBV waveforms were also fit, the analysis was done using the measured MKBV waveforms to change as few variables as possible to be sure that any changes were due to the modified MKBH damping. Furthermore the studies were done with the STD filling scheme as for the former analysis of energy deposition in the retrigger scenario this filling scheme was used too.

Here we studied only the behavior for modifying the damping of the MKBH waveforms as the generators for these magnets are currently being upgraded. Further analysis could still be done to investigate the effects of a higher attenuation of the MKBV waveforms, technically there are the same margins to change the damping. As for now there are no plans to change anything in the MKBV generators the effect of higher damping was not investigated for the vertical dilution. Still, the overlap that occurs around 5 µs and the one around 34 µs of retrigger time delay might be, for example, reduced with higher damping in the MKBV waveforms.

4.3.2 Analysis of the effect of higher damping in the retrigger scenario

The effect of higher damping was studied for the retrigger scenario for two reasons: First, for this scenario we can compare the maximum densities for a lot of different patterns and second, a higher damping is interesting for trying to avoid overlaps in the sweep pattern, a problem that can occur for some retrigger delay times.

As mentioned above, there are technical reasons that limit how much the damping can be increased. However, with the aim to understand properly the behavior of the patterns and the density under changing attenuation, a wide range of damping factors was investigated. MKBH waveforms with damping between 40 % and 81 % (this is the damping of the current MKBH waveforms) were created and their effects analyzed.

For all the implemented damping factors, the density and overlaps for all retrigger times were compared to the ones of the measured new MKBH waveforms. The densities for the newly generated waveforms with higher damping were normalized to the density of the nominal pattern of the measured new MKBH waveforms.

Studying these comparisons yields several results:

First, it was not possible to perfectly fit the measured MKBH waveforms due to the non sinusoidal ascent in the beginning and thus the errors for the studies with the increased damping should be considered to be higher. A doubled error as for the analysis with waveform data, thus four bunches, should be used here.

Secondly, it is confirmed that the overlaps are reduced when the damping is increased. For the US window, the overlap around 34 µs vanishes if the second maximum of the waveforms is at most 75 % of the first maximum, that is only 2 % more than with the measured ones. For this damping factor there is a small increase in density for the retrigger patterns around 71 µs: For these patterns the point of highest density is at the end of the sweep path and is thus due to low sweep velocity. As with higher damping the velocity at the end of the extraction decreases even more, the density increases. Still, for the 75 % of damping this density increase in the US window is within the error of four bunches. The 75 % damping looks promising for the US window, the overlap disappears and for no retrigger pattern there is a significant increase in density. It now has to be checked if that is also the case for the dump core and the DS window.

First of all, the effect on the density of changing the attenuation only a few percent is much less in these two locations than in the US window. So in general, there are no big changes in the density for the retrigger patterns at the dump core and the DS window for waveforms with 2 % more damping than the measured ones. Still, two changes can be observed: The peak around 5 µs gets more pronounced, but as stated before, this peak is always overestimated for these fitted waveforms. The other change is that the density increases slightly for late retrigger times due to slower velocity. These increases are more than the assumed error of four bunches but still lie below the worst case density of two missing MKBH. To have 2 % higher damping seems thus not to cause severe problems for the dump core and the DS window. The changes in the density and overlaps for a damping of 75 % can be observed in Figure 24.

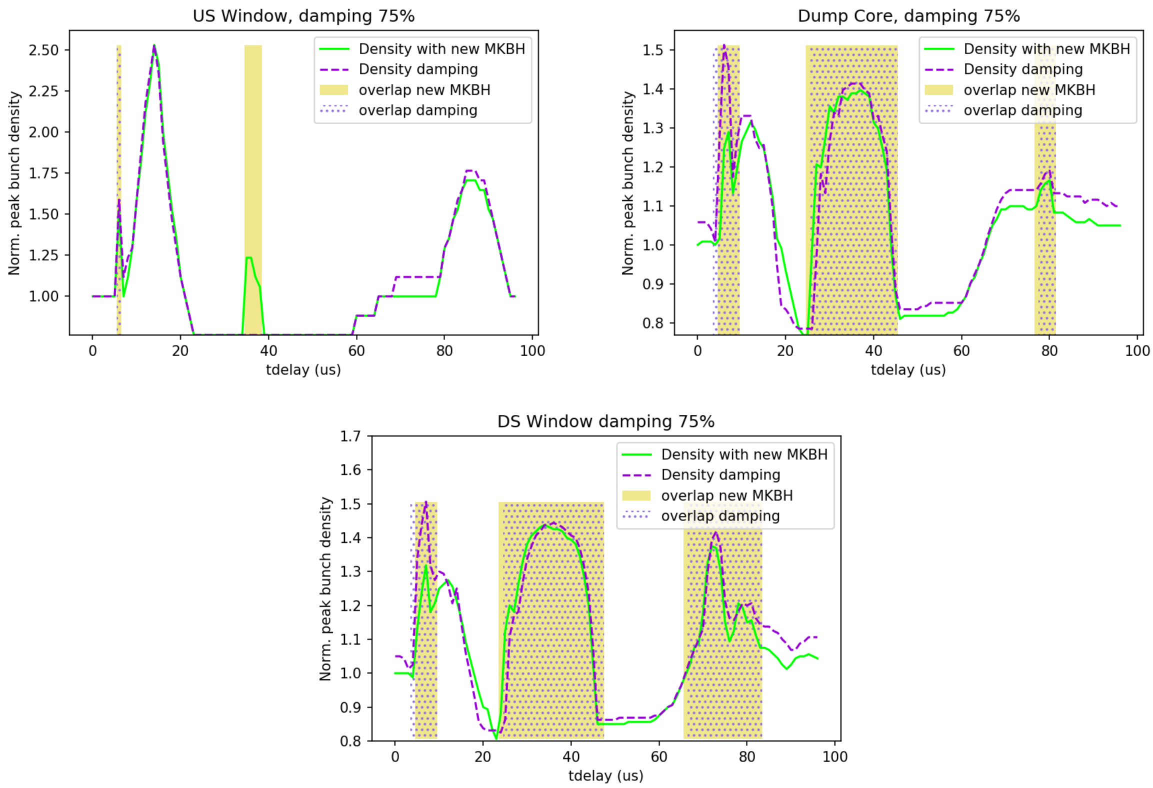

Figure 24: The effect on the density of increasing the damping of the MKBH waveforms by 2 % from 77 % to 75 % for all retrigger times

It was also investigated how much the damping has to be increased so that the overlap around 34 µs vanishes for the dump core or even for the DS window. For the core it disappears for a damping equal or bigger than 52 %. For the DS window a damping higher than 40 % would be needed. These are extremely high and unrealistic damping factors. Moreover, the density increases drastically for late retrigger times, as can be observed in Figure 25. So these extreme dampings would reduce overlaps but would increase the densities for late retrigger times. It is thus not realistic to try to get rid of all the overlap problems only with increasing the damping, at least if this is only done in one plane.

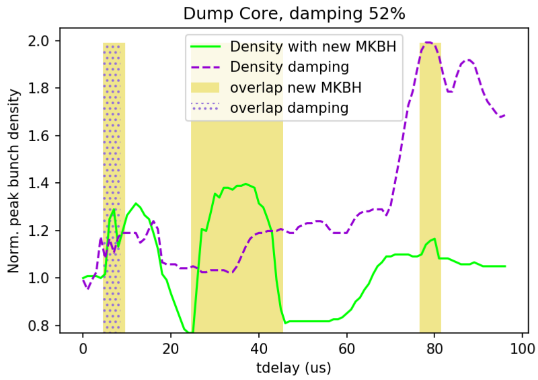

Figure 25: Effect of extremely high damping: No overlaps around 34 µs and around 86 µs in the dump core but large density increase for late retrigger times

4.3.3 Conclusion

The studies about increasing the damping of the MKBH waveforms leads the following results:

We can confirm that overlaps in the sweep path are reduced for a higher damping factor due to the fact that the path gets bent more to the inner part of the pattern because of less deflection. The downside of more attenuation is that the end part of the beam is swept with significantly lower velocity, which leads to higher density especially for late retrigger times.

Increasing the damping about 2 % to 75 % looks promising in the US window as the overlap around 34 µs vanishes and seems not to lead to major complications in the dump core or the DS window. Still, as there are significant density increases in terms of absolute numbers of bunch centers in the dump core and the DS window one could not draw the conclusion that 2 % more damping are beneficial in any case. But concerning a small increase of damping, it is good to know that the density will not change drastically with the damping varying around 1 % so even if there are slight changes on the magnet generator side, the energy deposition will not be extremely sensitive to that. However, the attenuation should not increase nor decrease more than 2 % as this would lead to higher densities.

For a general conclusion it can be said that the small increase of damping from the new waveforms is helpful, but it does not seem that even higher damping would lead to more improvement. A variation of around 1 % in the damping does not lead to major changes and would thus be acceptable.

4.4 Sensitivity studies: LHC filling scheme

4.4.1 Motivation and implementation of sensitivity studies

The dilution patterns are not composed of one solid line but of several chunks with gaps between them. These chunks are the result of the LHC filling scheme used during operation. Even if in the LHC there is one possible bunch position every 25 ns, there are free bunch positions after a certain amount of bunches due to the rise times of the injection kickers of the pre-accelerators (see 2.2). Thus, there are some constraints for the filling schemes but the exact position where the batches of bunches are placed and where the free spaces are are not fixed. By observing the various dilution patterns, it can be seen that at some points, where an overlap could occur or get larger (i. e. at 8 µs retrigger delay) or where the velocity is low (i. e. at 50 µs retrigger delay) we actually do not get a very high density because there are no bunches at these problematic spots in the used filling schemes. That means there might be the possibility to get significant increases in density if some slots were occupied, that now, just because of a specific filling scheme, were empty. This is why we have to investigate how sensitive the density is to a specific filling scheme. All the analyses are done with the new MKBH waveforms.

For the implementation, generic Standard and BCMS filling schemes are created. These created schemes respect only the absolutely necessary constraints of free gaps due to the PS and SPS injection kickers and are in all the rest as full as possible. Both filling schemes consist of trains of bunches of 288 batches. For the Standard filling scheme in one train there are four times 72 bunches, each batch of 72 bunches separated by 200 ns free gaps (for the injection to the SPS). For the BCMS filling scheme each train has six times 48 bunches[5], each batch of 48 bunches separated by 200 ns free slots (for the injection to the SPS). After each train there are 800 ns free for the injection from the SPS to the LHC. With this, we get for the Standard filling scheme 10 trains of 288 bunches, leading to a total of 2880 bunches in the LHC (the normal Standard filling scheme has 2760 bunches). For the BCMS filling scheme we get 9 trains of 288 bunches and 1 train of 144 bunches and a particle free region of 1000 ns, leading to a total of 2736 bunches in the LHC (the normal BCMS filling scheme has 2556 bunches). So we constructed generic filling schemes, respecting all constraints due to injection and thus being realistic, but that have more bunches than normally used. These schemes represent the highest possible density of bunches in the LHC with Standard and BCMS patterns.

As a first step, a precheck is done: To understand where possible density hotspots could be, the densities for a hypothetical full LHC, that is one bunch every 25 ns, are calculated. Figure 26 shows clearly that for the US window the density increases strongly at three peaks, whereas in the dump core and in the DS window the density increases for some retrigger times but is in general much less sensitive than in the US window. The sensitivity studies will thus be done in two parts: One for the US window and one for the DS window.

First, the method for the US window shall be explained. The three peaks, where the density increases for the US window, correspond to the retrigger patterns where the MKD work against the MKBH: The two peaks around 14 µs and 86 µs get much higher, and a new peak rises around 50 µs. As described in 4.1.2 at 50 µs the cancellation between the kickers leads to the beam going back and forth only twice (and not a triple superposition as for 14 µs and 86 µs). In the normally used filling schemes Standard and BCMS the density of bunches in this region is not high enough that this double superposition leads to an increased density. But having a full LHC, this cancellation between the kickers has a noticeable effect. Additionally to these peaks the density increases around 6 µs and 40 µs, that is the overlaps get larger. Observing the patterns corresponding to these high density regions, it is clear, that all these density increases are due to the fact that all the bunch positions in the very beginning and the very end of the LHC are filled (except the abort gap). This is why for studying a realistic worst case for the density in the US window, the two created generic filling schemes for Standard and BCMS are shifted in a way such that the very beginning and the very end of the slots are filled, leaving the abort gap empty as always. That means that the slots in the created generic Standard filling scheme are shifted 148 positions, and the slots in the created generic BCMS filling scheme are shifted 368 positions. With this shifting there is half a train in the beginning and half a train in the end having the very first and very last slots occupied. The filling schemes so obtained are considered to be the worst case filling schemes for the US window.

The approach for the DS window is different. Using the full LHC scenario, the density radius considered to represent the DS window contains at least 145 bunches whereas using the Standard filling scheme it contains at least 129. As explained above, it is unrealistic to have 145 bunches without free spots between each other, this is why using the Standard filling scheme this number reduces to 129. So the full LHC scenario is overestimating the density. By observing Figure 26 and investigating the corresponding patterns, for the DS window it is not as obvious as for the US window what leads to an increase of density. Therefore the approach here is different: For

[5]Even if the normal BCMS filling scheme has 3 batches of 48 bunches in one train it is technically feasible to have 6 batches in one train [9].

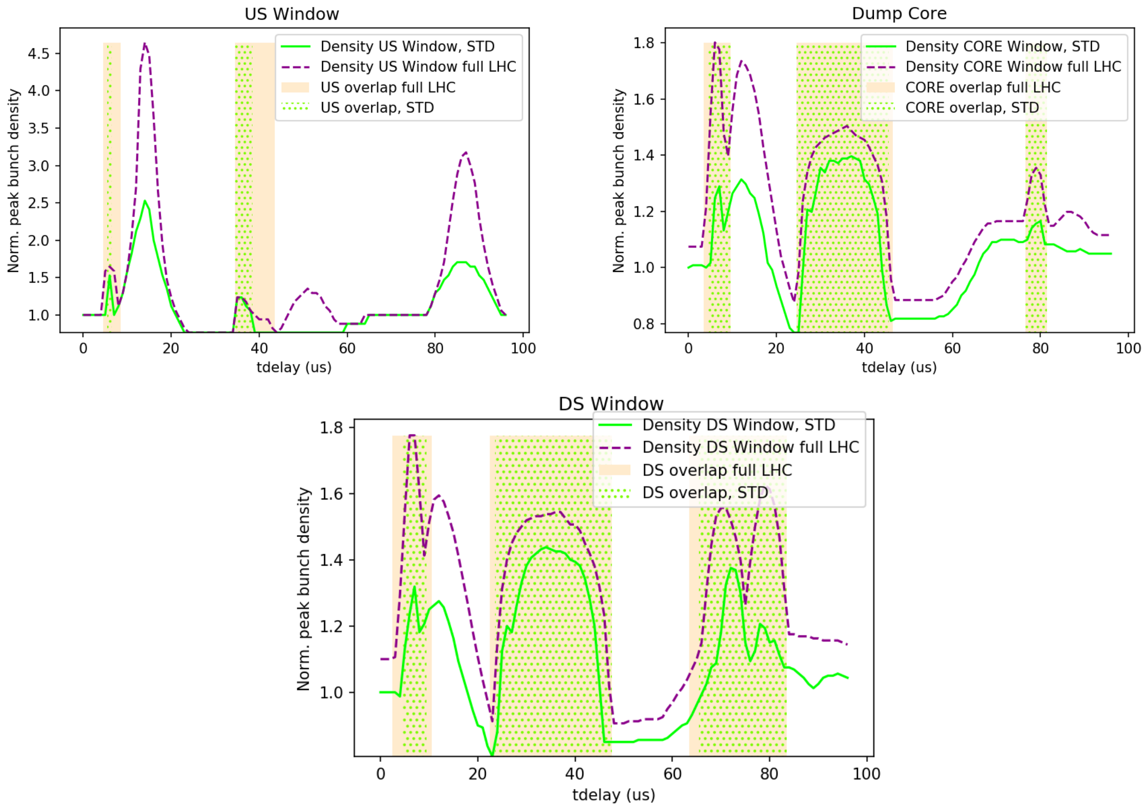

Figure 26: Density for a hypothetical filling scheme with every 25 ns slot in the LHC filled compared to the density obtained with the Standard filling scheme (Normalization to density of nominal pattern using the Standard filling scheme). All sweep patterns are calculated with the new MKBH waveforms

every retrigger pattern the point of highest density using the full LHC is calculated. The generic filling schemes constructed above are then shifted in a manner such that around this point of highest density the realistic maximum number of bunches is placed. With this, the density is re-calculated using these shifted generic Standard and BCMS filling schemes. That means for each retrigger pattern the filling schemes are shifted individually corresponding to the respective highest point of density.

As the changes in peak densities for the dump core using the full LHC scenario are similar to those for the DS window, the process is only done for the DS window and the results are considered to be valid also for the core. The DS window was chosen for the analysis as it is the other extreme to the US window and the biggest radius is used for its investigation, thus the free slots have more impact for the DS window than for the core as in a larger radius there could be more free slots.

4.4.2 Analysis of sensitivity of density in the retrigger scenario

For both windows even using worst case filling schemes, the maximum density does not change for the nominal pattern. It stays at 17 bunches for the US window and 176 bunches for the DS window in the corresponding radii.

For the US window, using the worst case filling schemes, that is filling schemes which have all slots occupied in the beginning and the end of the beam, the density increases for the same retrigger patterns as what was observed in the precheck for the hypothetical full LHC scenario: Figure 27 shows peaks around 6 µs, 14 µs, 34 µs, 50 µs and 86 µs retrigger delay time. The peaks are not as high as with the full LHC but still considerably higher than with the normal Standard filling scheme (the green curve). As expected, overlaps occur for more retrigger patterns than with the normal Standard filling scheme: The overlap regions around 6 µs and around 34 µs get more extended.

It can also be observed that for most peaks the density is higher for the Standard worst case filling scheme than for the BCMS worst case filling scheme. Only for the peak around 86 µs does the BCMS scheme lead to a worse effect.

For both worst case schemes, the peak densities for delay times around 14 µs and 86 µs are higher than the peak density for two MKBH missing, the assumed worst case.

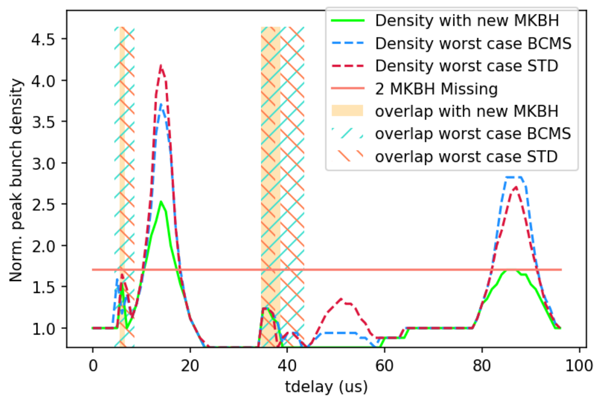

Figure 27: Peak densities in the retrigger scenario for worst case filling schemes in comparison to the normally used Standard filling scheme (green line) for the US window. All sweep patterns are calculated with the new MKBH waveforms

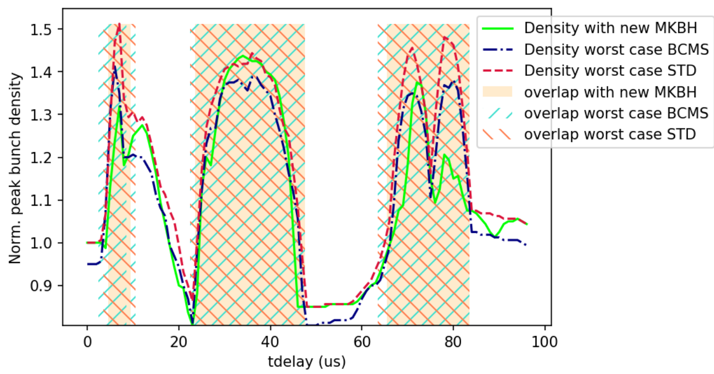

Figure 28: Peak densities in the retrigger scenario for worst case filling schemes in comparison to the normally used Standard filling scheme (green line) for the DS window. All sweep patterns are calculated with the new MKBH waveforms

The DS window is much less sensitive to the filling scheme than the US window (see Figure 28). The overlap regions around 5 µs and around 64 µs increase only marginally. Still, some peaks, mainly due to overlaps, increase significantly. It can be observed that the worst-case-BCMS filling has even lower maximum densities than the normally used Standard filling scheme. As the LHC is currently running most of the time with the BCMS filling scheme in most cases we are thus far away from a worst case scenario. For the retrigger scenario, the maximum of bunches in the radius corresponding to the DS window is 230 for the normally used Standard filling scheme, 226 for the worst-case-BCMS filling scheme and 242 for the worst-case-Standard filling scheme. The full LHC scenario returns 284 as the maximum number of bunches, which overestimated the maximal density in comparison with the worst-case-Standard filling scheme by around 17 %.

For all scenarios shown in Figure 28 the densities remain below the assumed worst case of two MKBH missing.

One curiosity happens for the retrigger pattern at 34 µs time delay for the DS window: Here the maximum density for the so called worst-case-Standard filling scheme shows 3 bunches less than the normal Standard filling scheme. This can be explained as follows: For the retrigger pattern at 34 µs there is a very broad region of high density (due to the overlap) with a high number of bunch center positions showing the same maximum density. For the sensitivity studies the generic filling schemes get moved to the first bunch center position with highest density. In this case this yields a small artefact because the density would increase a bit more if the filling scheme were to be moved a bit further into the dense region and not be placed at the first point with highest density. This occurs only for one pattern and as can be seen by observing the densities for the full LHC scenario (Figure 26) the sweep pattern at 34 µs delay time has a similar density to the retrigger patterns next to it. Thus this density will not change drastically even if it was studied separately, so it was decided that no special treatment needs to be done for this pattern.

4.4.3 Conclusion

The studies show that the US window is quite sensitive to a change in the filling scheme. Peaks of density would increase drastically if the very first and the very last bunch slots (always except the abort gap) were filled. For the retrigger patterns with the highest densities, at 14 µs and at 86 µs, the density would be increased by 65 % and 55 % respectively that is 145 % and 55 % more density than the assumed worst case of losing two MKBH. This has to be considered for the thermo-mechanical stresses of the US window, if one wants to keep the filling schemes fully flexible.

In contrast, the DS window is in general not very sensitive to changes in the filling scheme. However, some peak densities increase, particularly at 6 µs by 19 % and at 80 µs by 27 %.

For both windows it can also be observed that in almost all cases the peaks for the worst case Standard filling scheme are higher than for the worst case BCMS filling scheme. This can be explained by the fact that the BCMS trains are composed by six times 48 bunches whereas the Standard trains are composed by four times 72 bunches. That means the BCMS trains have more free bunch positions and thus the total density will in general be lower. Thus, for the retrigger scenario the BCMS filling scheme is less critical than the Standard filling scheme in terms of bunch densities. However, it has to be emphasized that the BCMS filling scheme uses a smaller emittance than the STD filling scheme. Previous studies showed that due to the fact that for the US window the local energy deposition is crucial, the BCMS filling scheme can lead to higher thermo-mechanical stresses than the STD filling scheme, as the smaller emittance means that the beam has a higher brightness [10]. For the US window this higher concentration of protons has a noticeable effect and can lead to higher stresses even if the BCMS filling scheme has more free bunch slots than the STD filling scheme. Hence, the bunch density can only be used as an indicator and for relative comparison but no final conclusion concerning the integrity of the dump or the absolute energy deposition can be drawn from it.

5 Conclusion

The LHC beam dump system is crucial for the protection of the accelerator. At any time during operation it has to be possible to safely extract and dump the proton beam. To lower the energy density at the graphite dump, the beam is swept over the front-face of the dump by a dilution system using fast-pulsed horizontal (MKBH) and vertical (MKBV) kicker magnets. For the High Luminosity LHC (HL-LHC) several upgrades to the beam dump system will be done that motivate this study. In this work, failure cases for the LHC beam dump dilution system, that is reduced dilution due to missing kickers (for example because of a flashover in the magnet tank) or erratic firing, were studied leading to the following results:

A new Python routine was developed to calculate the dilution patterns and estimate the proton bunch density at the dump. The patterns for the currently used kicker waveforms were benchmarked to an existing routine using beam transfer code [22] and the bunch density estimation was benchmarked to calculations for the energy deposition using FLUKA [7]. In this work one proton bunch was operationalized with one data point. That means the bunch intensity was not taken into account. Therefore all the analysis was done with normalized bunch densities. The method developed here of analyzing bunch densities thus yields no absolute values about the energy deposition but works very well for relative comparisons. Moreover, as stated in chapter 2.3, what determines the integrity of the dump are the thermo-mechanical stresses. The bunch density can only give indications of critical cases. More detailed thermo-mechanical-stress studies are needed to guarantee a safe operation of the beam dump system with HL beams. The bunch density was studied at the entrance of the dump, that is the upstream (US) window, inside of the graphite dump (the dump core) and at the end of the dump, that is the downstream (DS) window.

The creation of the dilution pattern was analyzed in detail. The form of the pattern, that is close to a spiral, is generated by the damped-sine magnetic fields of the four horizontal and six vertical dilution kickers that are shifted 90° to each other. The horizontal deflection of the extraction kickers (MKD) give a slight additional dilution.

From Run 3 of the LHC starting in 2021 on, as a mitigation strategy against the risk of erratic firing of dilution kickers a retrigger system will be implemented. It implies that all other kickers are fired in case one (ore more) kickers prefire. This leads to changes in the dilution pattern depending on the delay between the firing of the dilution kickers and the start of the extraction. In some cases the bunch density at the dump increases strongly. These increases are mainly due to two reasons: A very low sweep velocity or an overlap of the dilution path.

Also from Run 3 on, the generators for the horizontal dilution kickers are upgraded. This leads to a slight change in their waveforms giving them an increase of damping of 3 %. For these new waveforms the implications for nominal dilution and the failure cases were investigated.

The bunch densities for the nominal dilution and the failure case of reduced dilution due to missing MKB remain within error bars the same as for the currently used waveforms. In none of the studied cases does the dilution get worse in the retrigger scenario when compared to the current waveforms. In some cases the density can be reduced. This occurs mainly because of less overlaps due to higher damping in the waveforms.

As the higher damping of the new MKBH waveforms lead to positive results for the retrigger scenario, in a next step it was investigated whether even higher damping would reduce the density even more. By increasing the damping only 2 %, the overlaps in the US window vanish. However, these modified waveforms would lead to slight increases of the density in the dump core and the DS window. In general, the studies of modifying the damping factor of the horizontal dilution kickers give as a result that an even higher damping is not beneficial due to the fact that the end part of the beam would be swept with a lower velocity which will be even more noticeable for large retrigger times. However, if due to technical issues the damping should increase or decrease by 1 % this does not have major implications for the bunch density and would be acceptable without further studies.

In the end it was studied how sensitive the bunch density is to the LHC filling scheme. Due to the rise time of the injection kickers of the pre-accelerators there are gaps between the batches of proton bunches in the LHC but the exact positions of these free spots is not fixed. The aim was thus to investigate the dependence of the density to the positions of the particle free gaps. The result is that in the US window, where the particles directly impact, the density varies strongly for certain changes in the filling schemes: The density can increase by a maximum of 65 % for some retrigger times if all possible bunch positions at the beginning and the end (except the particle free region of the abort gap) of the LHC are filled. At the dump core and the DS window the density is not very sensitive to changes in the filling scheme. A maximum increase of 27 % can be observed for the worst-case filling schemes studied.

In this work, the dependence of the damping of the waveforms was only investigated for the horizontal kickers. Further studies could investigate the effect of higher damping in the vertical kickers. It might be possible to reduce overlaps in the retrigger scenario but still not lower the sweep velocity too much if both dilution kicker waveforms would get their damping increased slightly.

Within this thesis, Python code was developed to analyze the patterns and proton bunch densities. It is available as a Jupyter notebook on the CERN SWAN network and can be used for further analysis of dilution patterns given specific waveforms or if dilution patterns are already given their densities and overlaps may also be analyzed with a dedicated script.

6 Acknowledgements

First of all I am profoundly grateful for all the help and support I got from my supervisor at CERN, Dr. Christoph Wiesner. Whatever was my question there was a time to discuss it. With him, all the Accelerator Beam Transfer (ABT) group at CERN was very helpful and it was an incredible environment to learn and work. I also would like to thank my supervisor at Leibniz University Hannover, Prof. Dr. Christian Ospelkaus, for his great flexibility and advice without which this thesis would not have been possible. My sincere thanks go to Linda Stoel and Javier Prieto Prieto for their great advice with programming problems and to Rafael Maldonado for extremely helpful comments on my writing. I also would like to thank Dr. Michael Flohr from Leibniz University Hannover. Without his encouraging support during many years I would not have gone to participate in the CERN Summer Student Programme what in the end lead to this thesis.

Heartfelt thanks go to my friends and family for warm motivation and support. Especially my grandmother Ursula Schreiber made me feel very well in a difficult episode.

7 Appendix

7.1 Benchmarking

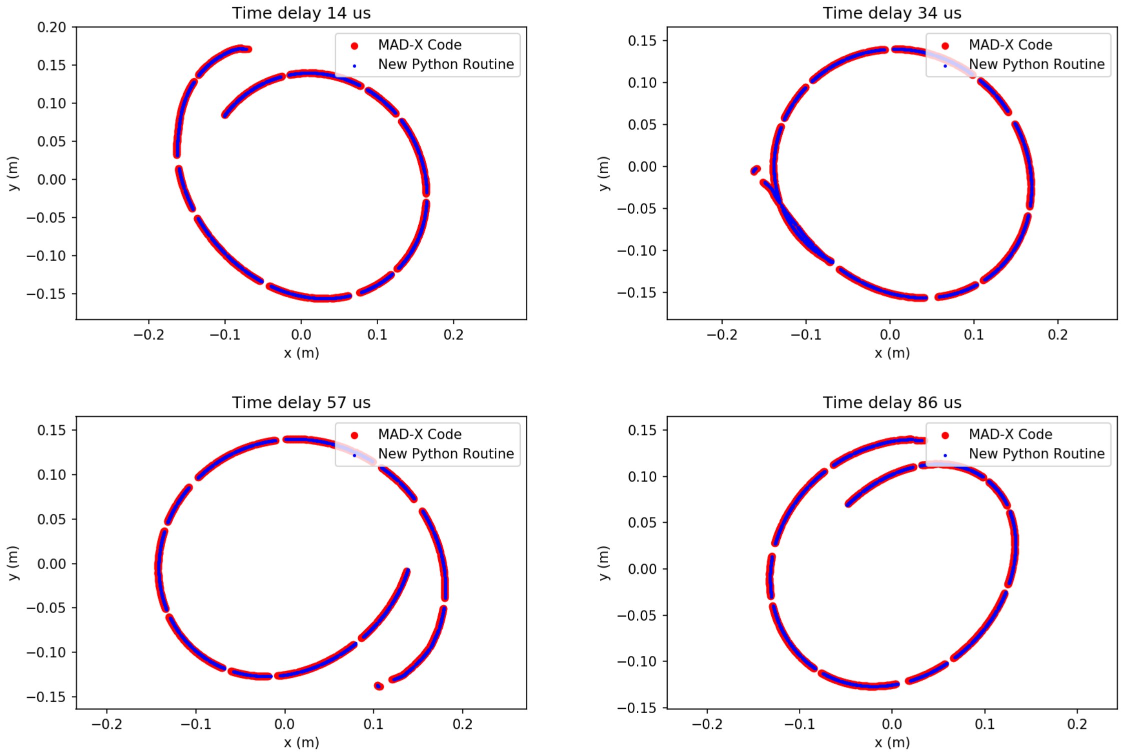

Figure 29: Comparison of the patterns calculated with the new Python routine used in this thesis with the patterns calculated with beam transfer code (MAD-X) for selected retrigger times

7.2 Missing MKB

Number of active MKBH \ Number of active MKBV	6	5	4	3	2	1	0
4	100	102	106	134	188	280	418
3	130	130	130	138	196	303	493
2	175	178	182	186	208	337	605
1	253	259	259	268	339	447	880
0	398	439	499	631	884	1330	2346

Table 5: *Estimated proton bunch densities in percentage of nominal dilution for different number of active MKB kickers at dump core for current MKBH waveforms*

Number of active MKBH	Number of active MKBV: 6	5	4	3	2	1	0
4	100	101	104	132	181	275	418
3	126	126	128	135	189	295	492
2	173	176	180	183	204	330	589
1	248	253	253	263	338	442	961
0	388	427	486	614	861	1295	2284

Table 6: *Estimated proton bunch densities in percentage of nominal dilution for different number of active MKB kickers at dump core for new MKBH waveforms*

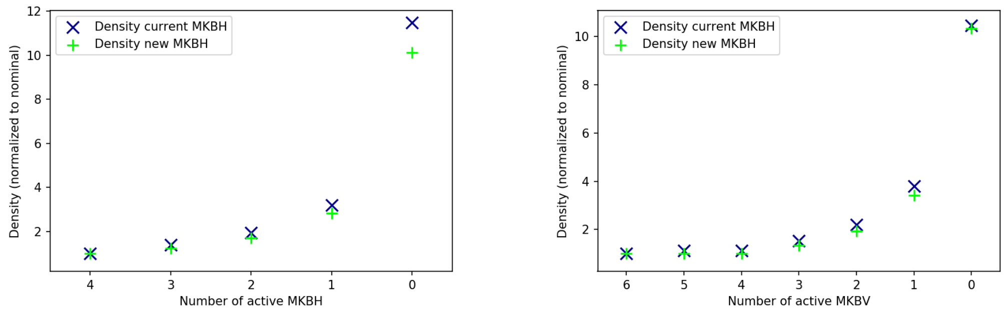

(a) *Missing MKBH* (b) *Missing MKBV*

Figure 30: Comparison of increase of bunch density for current and new MKBH waveforms at the US window for missing dilution kickers

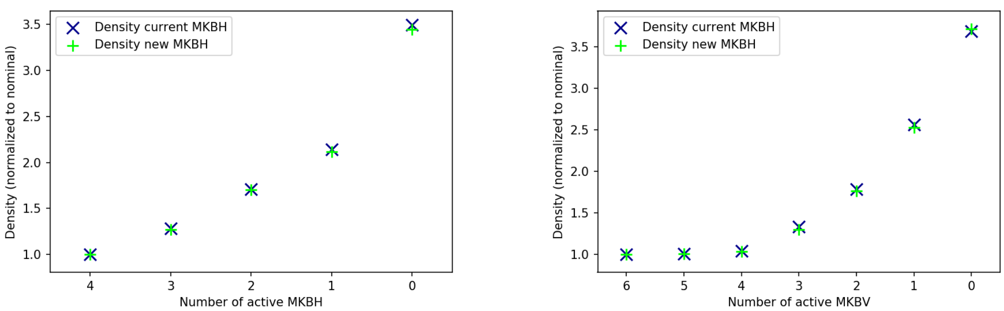

(a) *Missing MKBH* (b) *Missing MKBV*

Figure 31: Comparison of increase of bunch density for current and new MKBH waveforms at the DS window for missing dilution kickers

8 Literature

References

[1] Giorgio Apollinari, Oliver S. Brüning, Tatsushi Nakamoto, and Lucio Rossi. High Luminosity Large Hadron Collider HL-LHC. *CERN Yellow Report CERN-2015-005*, 2017.

[2] Chiara Bracco. LBDS and injection system, 2016 (accessed October 25, 2018). https://indico.cern.ch/event/448109/contributions/1942027/attachments/1217299/1782246/LBDSInjection_Chamonix2.pdf.

[3] Oliver S. Brüning, John Poole, Paul Collier, Philippe Lebrun, Ranko Ostojic, Stephen Myers, and Paul Proudlock. LHC design report, 2004.

[4] Luca Bruno and Serge Péraire. Design studies of the LHC beam dump. Technical report, CERN-LHC-Project-Note-196, 1999.

[5] CERN. Project schedule, 2018 (accessed October, 29, 2018). https://project-hl-lhc-industry.web.cern.ch/content/project-schedule.

[6] Alessandro Dallocchio. *Study of thermo-mechanical effects induced in solids by high energy particle beams: analytical and numerical methods.* PhD thesis, Turin Polytechnic, 2008.

[7] Matthias Frankl. Temperature estimates for the external LHC beam dumps (TDE), 2017 (accessed November 2, 2018). https://indico.cern.ch/event/647714/contributions/2646292/attachments/1558138/2451898/TDE_HL-LHC.pdf.

[8] Giovanni Iadarola, Lotta Mether, and Giovanni Rumolo. Filling schemes and e-cloud constraints for 2017. In *Proc. of the 7th Evian Workshop, Evian*, pages 13–15, 2017.

[9] Giovanni Iadarola and Giovanni Rumolo. Filling schemes and e-cloud constraints, 2016, (accessed October 27, 2018). https://indico.cern.ch/event/578001/contributions/2367030/attachments/1388974/2115360/010_ecloud_session8.pdf.

[10] Anton Lechner. Energy deposition studies for extraction protection devices (TCDQ, TCDS) and the beam dump (TDE), 2018 (accessed October 24, 2018). https://indico.cern.ch/event/742082/contributions/3085168/attachments/1736574/2808967/2018_18_10_extractionenergydep.pdf.

[11] Michael Monteil. Etude thermo-elastique de la fenetre du dump, 2010 (accessed October 24, 2018). https://edms.cern.ch/ui/#!master/navigator/document?D:1435007425:1435007425:subDocs.

[12] Tobias Polzin. Updates on the thermo-mechanical studies of the TDE dump block assembly, 2018 (accessed October 24, 2018). https://indico.cern.ch/event/742082/contributions/3085169/attachments/1736613/2809718/HiLumi_TDE_8thCollaborationMeeting.pdf.

[13] Viliam Senaj. The LHC beam dump system for 7.5 TeV, 2018 (accessed November 27, 2018). https://indico.cern.ch/event/676124/contributions/2768631/attachments/1593350/2522515/LBDS_at_7.5_TeV.pdf.

[14] Viliam Senaj. Measurement of the MKBH waveforms with higher capacitance, August, 31, 2018. Private Communication.

[15] Viliam Senaj. Simulation of the MKBH waveforms with higher capacitance, July, 31, 2018. Private Communication.

[16] Viliam Senaj. Simulation of damping factor, October, 19, 2018. Private Communication.

[17] Naeem Ahmad Tahir, J. Blanco Sancho, Alexander Shutov, Rüdiger Schmidt, and A. Roberto Piriz. Impact of high energy high intensity proton beams on targets: Case studies for super proton synchrotron and large hadron collider. *Physical Review Special Topics-Accelerators and Beams*, 15(5):051003, 2012.

[18] Helmut Wiedemann. *Particle Accelerator Physics*. Springer International Publishing, Heidelberg New York Dordrecht London, 2015.

[19] Christoph Wiesner. Failures cases for the LHC dilution system, 2018 (accessed October 25, 2018). https://indico.cern.ch/event/747908/contributions/3093467/attachments/1722047/2780607/2018-09-25_ABTEF_MKB_failures.pdf.

[20] Christoph Wiesner. MKB re-triggering: motivation, technical implementation, reliability analysis and expected energy deposition on dump block as function of triggering delay between MKBs and MKDs, 2018 (accessed October 25, 2018). https://indico.cern.ch/event/724736/contributions/2981141/attachments/1641036/2620626/2018-04-27_MPP_MKB_retriggering.pdf#search=mppapril2018wiesner.

[21] Christoph Wiesner. MAD-X Twiss File, August, 31, 2018. Private Communication.

[22] Christoph Wiesner, Matthew Fraser, Matthias Frankl, Nicolas Magnin, Malika Meddahi, Chiara Bracco, Thomas Kramer, Brennan Goddard, Wolfgang Bartmann, Viliam Senaj, et al. LHC beam dump performance in view of the high luminosity upgrade. Proceedings of IPAC 2017, Copenhagen, Denmark, WEPIK033, http://accelconf.web.cern.ch/AccelConf/ipac2017/papers/wepik033.pdf.

[23] Klaus Wille. *Physik der Teilchenbeschleuniger und Synchrotronstrahlungsquellen*. Vieweg+Teubner Verlag, Wiesbaden, 1992.

[24] Jan M. Zazula. On graphite transformations at high temperature and pressure induced by absorption of the LHC beam. Technical report, CERN-LHC-Project-Note-78, 1997.

[25] Jan M. Zazula and Serge Péraire. LHC beam dump design study; 1, simulation of energy deposition by particle cascades; implications for the dump core and beam sweeping system. Technical report, CERN-LHC-Project-Report-80, 1996.

Versicherung
Hiermit versichere ich, dass:

- die Arbeit selbstständig verfasst wurde
- keine anderen als die angegebenen Quellen und Hilfsmittel benutzt wurden
- alle Stellen der Arbeit, die wörtlich oder sinngemäß aus anderen Quellen übernommen wurden, als solche kenntlich gemacht sind
- die Arbeit in gleicher oder ähnlicher Form noch keiner Prüfungsbehörde vorgelegen hat

Hannover, 29.11.2018

Lea Richtmann